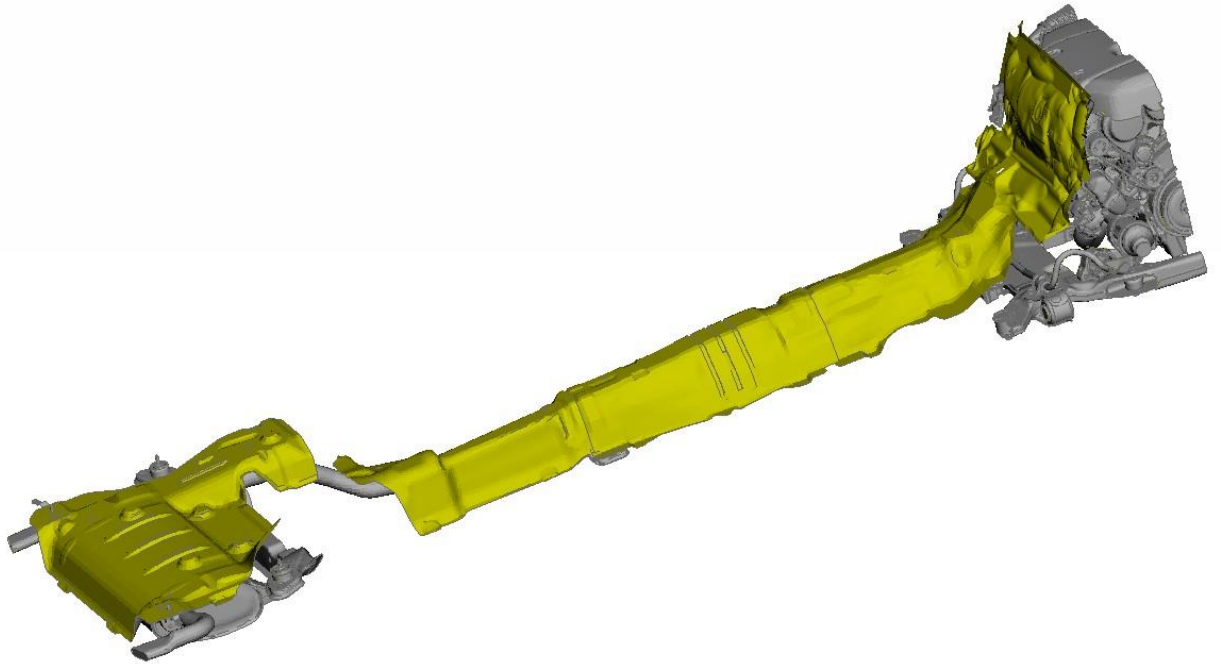




CHALMERS
UNIVERSITY OF TECHNOLOGY



Thermal Contact Resistance: Experiments and Simulation

Master's thesis in Automotive Engineering

Karthik Narendra Babu

MASTER'S THESIS IN AUTOMOTIVE ENGINEERING

**THERMAL CONTACT RESISTANCE:
EXPERIMENTS AND SIMULATIONS**

Karthik Narendra Babu

Department of Applied Mechanics
Vehicle Engineering and Autonomous Systems
Vehicle Aerodynamics and Thermal Management
CHALMERS UNIVERSITY OF TECHNOLOGY
Göteborg, Sweden 2015

THERMAL CONTACT RESISTANCE: EXPERIMENTS AND SIMULATIONS
Karthik Narendra Babu

© Karthik Narendra Babu, 2015-06-06

Master's Thesis 2015:07
ISSN 1652-8557
Department of Applied Mechanics
Vehicle Engineering and Autonomous Systems
Vehicle Aerodynamics and Thermal Management
Chalmers University of Technology
SE-412 96 Göteborg
Sweden
Telephone: + 46 (0)31-772 1000

Cover:
The model for the complete engine bay and exhaust system

Department of Applied Mechanics
Göteborg, Sweden 2015-06-06

THERMAL CONTACT RESISTANCE: EXPERIMENTS AND SIMULATIONS

Master's thesis in Automotive Engineering

Karthik Narendra Babu

Department of Applied Mechanics

Vehicle Engineering and Autonomous Systems

Vehicle Aerodynamics and Thermal Management

Chalmers University of Technology

Abstract

The engine bay and exhaust system of modern day vehicles consists of components, made out of different materials with different thermal conductivities. The heat transfer across the interface between two components in contact with each other is significant to determine their surface temperatures. This phenomenon becomes more critical for components which are made from materials with a lower thermal conductivity.

The effect of thermal contact resistance on the surface temperatures of these components is analysed. Different parameters that affect the value are studied and their values are determined from literature.

Component level analysis is carried out using physical tests and simulations. The complete vehicle simulation was then carried out by coupling thermal simulations with a CFD code. The critical components which were affected by thermal contact resistance were identified in the engine bay and exhaust system.

A method to estimate the value of contact resistance was developed based on material properties. A simulation was run with the estimated values of contact resistance and the results were found to correlate better to wind tunnel tests.

Key words: Thermal Contact Resistance, CFD

Contents

Abstract.....	I
Contents.....	III
Acknowledgement.....	V
Notations.....	VI
1 Introduction.....	1
1.1 Background.....	1
1.2 Objective.....	1
2 Theory.....	2
2.1 Heat Transfer.....	2
2.1.1 Thermal Conduction.....	2
2.1.2 Thermal Convection.....	3
2.1.3 Radiation.....	3
2.2 Thermal Contact Resistance.....	4
2.3 Factors affecting Thermal Contact Resistance.....	5
2.3.1 Micro-Hardness of the material.....	6
2.3.2 Contact Pressure.....	6
2.3.3 Surface Roughness.....	6
2.3.4 Thermal Conductivity of the Materials.....	6
2.3.5 Asperity Slope.....	6
2.4 Theories to predict Thermal Contact Resistance.....	6
2.4.1 Basic Relations.....	7
2.4.2 Elastic Models.....	7
2.4.3 Plastic Models.....	8
2.5 Treatment of oxidised surfaces.....	9
2.6 Treatment of welded surfaces.....	10
2.7 Parametric Study.....	11
3 Procedure.....	12
3.1 Sensitivity Analysis.....	12
3.2 Experimental Setup.....	12
3.3 Simulation Setup.....	14
3.3.1 CAD Cleaning.....	14
3.3.2 Meshing.....	14
3.3.3 Thermal Model Setup.....	15
3.4 Coupling Thermal Simulations with a CFD Code.....	15

4	Results and Discussion.....	16
4.1	Results from the Parametric Study.....	16
4.2	Results from the Sensitivity Analysis	17
4.3	Component Analysis.....	18
4.3.1	Downpipe and Exhaust Hanger.....	18
4.3.2	Manifold Heat Shield	23
4.3.3	Powertrain Mounts	27
4.3.4	Full Vehicle Simulation.....	29
5	Conclusion and Scope for Future Work.....	33
6	References.....	34
	Appendix A	35
	Appendix B	39
	Appendix C.....	40
	Appendix D	42
	Appendix E.....	43

Acknowledgement

The thesis work was carried out in Volvo Car Corporation at the ‘Thermodynamics Department’ in coloboration with the Applied Mechanics department at Chalmers Univeristy of Technology.

I would like to thank my supervisor Begoña León Moya for her able guidance and support throughout the project. Your inputs were key in shaping the outcomes of my thesis. I would also like to thank Prof. Lennart Löfdahl for his support throughout the thesis.

I am very grateful to the department of Thermodynamics at VCC for making the work environment so comfortable for me. I would like to thank the mechanics at the PVT workshop at VCC for their help during the experiments.

Finally, I would like to thank my parents for giving me the opportunity to come to Sweden and learn and develop both technically and as an individual.

Göteborg March 2015-06-06

Karthik Narendra Babu

Notations

Parameter	Description	Unit
q_x	Heat Transfer in the x- direction	W/m ²
k	Thermal Conductivity	W/ m K
α	Heat Transfer Co-efficient	W/m ² K
σ	Stefan Boltzman Constant	W/m ² K ⁴
R _c	Thermal Contact Resistance	W/m ² K
K _s	Effective Thermal Conduitivity	W/ m K
σ_s	Effective Surface Roughness	μm
m _s	Effective mean asperity slope	
h _c	Thermal Contact Conductance	m ² K/W
P	Contact Pressure	MPa
E'	Effective Elastic Modulus	MPa
ν	Poisson Ratio	
H _c	Micro-Hardness	MPa
R _s	Spreading Resistance	W/m ² K
CFD	Computational Fluid Dynamics	

1 Introduction

1.1 Background

The engine bay and exhaust system of modern day vehicles consists of components made out of different materials with different thermal conductivities. The heat transfer across the interface between two components in contact with each other is significant, to determine their surface temperatures. This phenomenon becomes more critical for components which are made of materials with a lower thermal conductivity. Many components made of materials with a low thermal conductivity, are mounted in hot parts of the engine bay. The heat balance determines its temperature. It is needed to secure the appropriate cooling of the components during its operation. To do so, one needs to engineer efficient cooling of a series of limited regions of the engine bay.

The challenge lies in the temperature difference that inherently appears at each interface. It is often referred to as contact resistance. The origin of the phenomenon is complex and is explained by non-perfect matching interfaces at microscopic levels. Without a clear theory to estimate the contact resistance, experiments are a key tool for tackling this problem.

This master thesis has been carried out in co-operation with Volvo Car Corporation in the Thermodynamics Department.

1.2 Objective

The objective of the thesis is to develop a method to estimate the **thermal contact resistance (R_c)** between different components in the engine bay and exhaust system.

The method is developed by combining physical tests carried out on individual components, with simulations in Radtherm™.

The obtained values of thermal contact resistance will then be input into a full car simulation, to study the effect of the parameter in determining the surface temperatures of different components of the engine bay and exhaust system.

2 Theory

This chapter will present the findings from the literature study. The basic theory of Thermal Contact Resistance (R_c) will be presented, which will be followed by the different models to predict the value of R_c . Then the different factors affecting R_c will be discussed with the help of some correlations. Finally, the effect of oxidation and welding on the value of R_c will be discussed briefly.

2.1 Heat Transfer

Heat transfer can be explained as transfer of energy from one medium to another due to a difference in temperature. According to the second law of thermodynamics, heat transfer is always in the direction of the falling temperature.

Heat transfer can occur in three modes: Conduction, Convection and Radiation.

2.1.1 Thermal Conduction

Conduction is the process of energy transfer between adjacent molecules due to the presence of a temperature gradient. The heat transfer exists until the system reaches an equilibrium. The heat transfer through conduction is governed by Fourier's law of conduction.

$$q_x = -k \frac{dT}{dx} \quad (1)$$

The term 'k' in the equation (1) represents the thermal conductivity of the material of study. It determines how much heat can be transmitted through the material. The heat flux per unit area in the equation (1) is proportional of the temperature gradient and the negative sign is due to the direction of heat transfer in the medium.

Figure 2.1 shows the visualization of heat transfer through conduction. Here the thermal conductivity and surface area is assumed to be constant. The heat flow is assumed to be one-dimensional. [1]

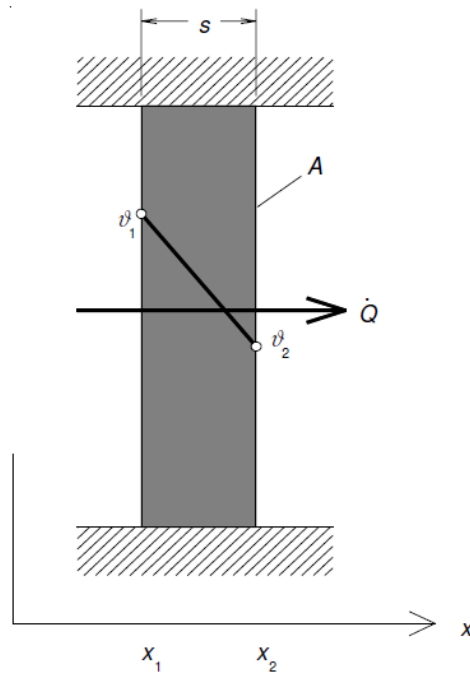


Figure 2.1 Heat Transfer through Conduction [1]

2.1.2 Thermal Convection

Convection is the mode of heat transfer where the energy is transferred due to macroscopic motion of fluid molecules. There are two kinds of convection: natural and forced convection.

Natural convection occurs due to an inherent temperature gradient. This temperature gradient induces a density difference in the fluid and due to the effect of gravity, the fluid with the higher density moves downward. Forced convection however, is setup using an external force or pressure difference. The convective heat transfer on a body is governed by the equation:

$$Q_x = \alpha A(T_2 - T_1) \quad (2)$$

Here the heat transfer depends on the temperature difference, the contact area and the heat transfer co-efficient.

2.1.3 Radiation

Radiation is the mode of heat transfer that does not depend on a medium for the heat transfer to take place. The energy is transmitted from an object in the form of electromagnetic waves. The heat transfer through radiation can take place even in vacuum.

When radiation is incident on a body a part of the energy is absorbed and a part of it is either absorbed or reflected. The energy which is absorbed causes the internal energy of the object to rise and consequently, the temperature of the object also rises. For gases and liquids radiation is a volumetric phenomenon. But in solids the absorption and the

emission are limited to a very thin layer close to the surface. So radiation in solids can be approximated to a surface phenomenon. [1]

The heat transfer due to radiation is governed by the equation:

$$q_x = \varepsilon \sigma T^4 \quad (3)$$

The effects of radiation become significant when the temperatures are high. An ideal body that can absorb all the incident radiation is called a black body. All real objects absorb a fraction of the heat that a black body absorbs at a given temperature called emissivity.

2.2 Thermal Contact Resistance

Although most surfaces seem flat in reality, on a microscopic level all of them are found to possess micro asperities. This effectively reduces the contact area when two surfaces are in contact with each other. The real contact area is found to be a small portion of the apparent contact area. The real contact area is dependent on many physical factors of the surface. The different factors effecting the contact area between the two surfaces are discussed in 2.3.

Figure 2.2 shows the microscopic view of an interfaee.

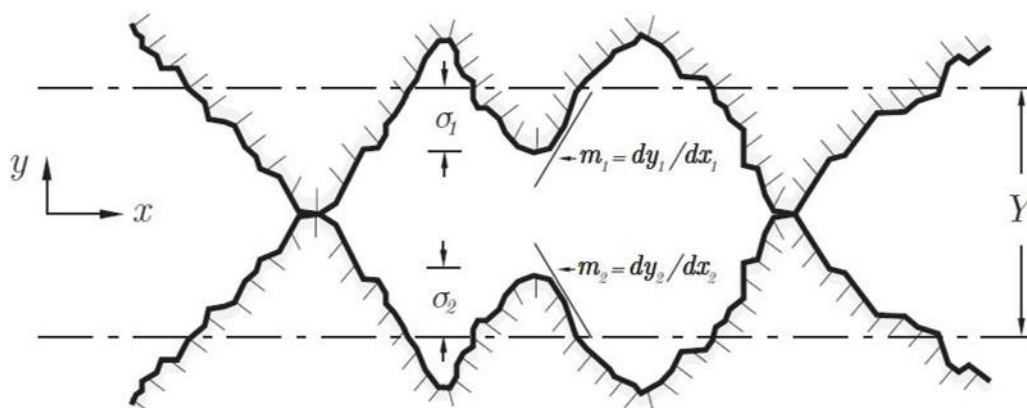


Figure 2.2 Microscopic view of two surfaces in contact [2]

This change in the contact area causes a drop in temperature across an interface, due to a decrease in the amount of heat that can be transferred across it. The drop in temperature is proportional to the value of thermal contact resistance which acts at the interface. It can be formulated as [2]

$$R_c = \frac{\Delta T}{Q} = \frac{\Delta T}{qA} \quad (4)$$

The reciprocal of thermal contact resistance is termed as thermal contact conductance.

Figure 2.3 shows the temperature profile at an interface. The heat transfer across the interface can occurs through all the three modes of heat transfer: Conduction, Convection and Radiation. [2]

$$h_j = h_c + h_g + h_r \quad (5)$$

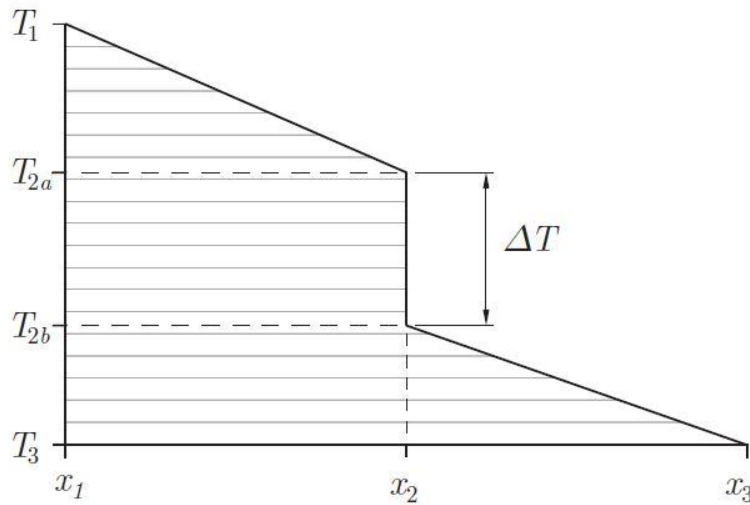


Figure 2.3 Temperature profile at the contact interface[2]

The effects of convective and radiative heat transfer at the interface present a low contribution to the heat transfer in comparison to conduction, and for most practical cases they can be neglected. For studies involving high accuracy the measurements are carried out in vacuum to completely eliminate the effects of convection. But, in this thesis due to the unavailability of resources the components were insulated from the environment to minimise the effects of convection.

2.3 Factors affecting Thermal Contact Resistance

Thermal contact resistance is affected by numerous physical factors depending on the two materials in contact. These factors discussed in this section have been listed in [2].

Figure 2.4 shows the effect of hardness and contact pressure at the interface, on the value of thermal contact resistance.

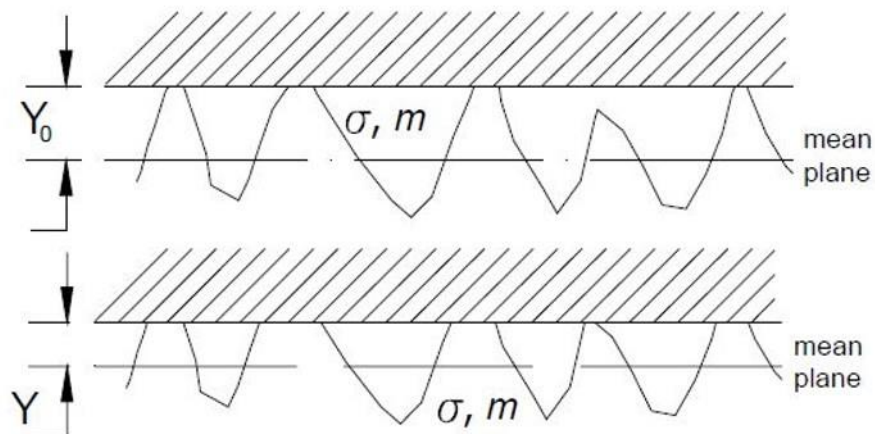


Figure 2.4 Visualisation of the effects of hardness and contact pressure at an interface

2.3.1 Micro-Hardness of the material

Microhardness of the material plays an important role in determining the value of the contact resistance at the interface. Figure 2.4 shows two materials, with different values off micro-hardness. The material on the top is harder than the material at the bottom. The deformation of the asperities of a harder material will be smaller, which reduces the contact area and increases the thermal contact resistance.

2.3.2 Contact Pressure

The contact area at the interface is proportional to the pressure acting on the surfaces. Figure 2.4 shows two different values of contact pressures acting on an interface. The contact pressure on the interface at the top is lower, than the contact pressure at the bottom interface. As the pressure increases the value of R_c decreases due to increase in the contact area for conduction.

2.3.3 Surface Roughness

An ideal smooth surface has 100% contact at the interface. But in reality even for highly polished surfaces it is very unlikely to obtain this condition. As the surface roughness increases the contact area reduces and consequently the value of R_c increases.

2.3.4 Thermal Conductivity of the Materials

A material with a higher value of conductivity will conduct more heat. As the value of thermal conductivity of the two materials at the interface increases the value of R_c decreases.

2.3.5 Asperity Slope

If the surface contains asperities with high slope values, the contact area is reduced and correspondingly the value of R_c increases.

By varying these parameters the thermal contact resistance can be modified at the interface.

2.4 Theories to predict Thermal Contact Resistance

Extensive studies have been carried out to quantify the numerical value of R_c . Over the years various models have been developed based on different input parameters. The different models are classified based on, if the deformation of the micro contacts are considered to be plastic or elastic in nature.

The real contact area is proportional to the applied load, which implies that the deformation is plastic in nature. All earlier theories were hence formulated based on the assumption that the deformations were plastic in nature and they did not account for the elastic deformations beneath the surface. This approximation is accurate if the elastic moduli of the contacting bodies were infinity or if the distances between the micro contacts were small such that the elastic deformation on both the micro contacts were the same. But, these assumptions are not true for most practical cases. [3]

At an interface each asperity can be considered as a micro indenter on the softer material. The pressure applied hence becomes effectively the micro hardness of the contact. At the point of contact the area is very small and therefore, the stress is higher than the yield stress of the material. This causes the deformation to be plastic in nature. But, at points slightly further away the stresses are lower and do not exceed the yield stress of the material. Therefore, there is a region of plastic deformation surrounded by regions of elastic deformation. This region of elastic deformation causes the gap thickness to reduce and more micro contacts are formed that causes R_c to decrease. [3]

Some of the models used to calculate the numerical value of R_c are presented below:

2.4.1 Basic Relations

There are some formulae which have been developed for certain parameters, which are used extensively for the estimation of R_c .

The effective thermal conductivity of the interface of two different materials is given by: [2, 5]

$$K_s = \frac{2K_1K_2}{K_1 + K_2} \quad (6)$$

The asperity slope and surface roughness values can vary locally on the surface. Therefore, it is needed to calculate the RMS (Root Mean Square) value of these parameters.. The rms Value of surface roughness and asperity slope at an interface is given by: [2, 3]

$$\sigma_s = \sqrt{\sigma_1^2 + \sigma_2^2} \quad (7)$$

$$m_s = \sqrt{m_1^2 + m_2^2} \quad (8)$$

2.4.2 Elastic Models

This section discusses the models which consider the deformation of the asperities to be elastic in nature.

Greenwood and Williamson model

Greenwood and Williamson proposed that for elastic deformation the contact area is not always linearly proportional to the load like in the case of plastic deformation. They proposed that in case of elastic deformation if the number of micro-contacts remain the same then the contact area follows the relation $A \propto F^{\frac{2}{3}}$. But if the increase in the load causes more micro-contacts to be nucleated then the relation becomes linear and $A \propto F$. Greenwood and Williamson also formulated a parameter called the plasticity index $((E' / H_c)(\sigma_s / \beta)^{\frac{1}{2}})$ [4] which is the ratio of the elastic hardness to the real hardness.

It is used as a criterion for plastic flow of asperities. If the plasticity index is high, then the asperities deform plastically. If the plasticity index is small, then the asperities deform elastically.[3, 4]

Here E' is the effective elastic modulus, H_c is the micro hardness of the material and β is the radius of the asperity which is assumed to be constant for all the asperities.

Mikic model

Mikic derived an expression for thermal contact conductance based on the material properties. The theory is formulated as : [2, 6]

$$h_c = 1.55 \frac{k_s m_s}{\sigma_s} \left(\frac{P \sqrt{2}}{E' m_s} \right)^{0.94} \quad (9)$$

The effective elastic modulus is given by:

$$\frac{1}{E'} = \frac{1 - \nu_1^2}{E_1} + \frac{1 - \nu_2^2}{E_2} \quad (10)$$

Mikic also formulated the plasticity index ($H_{mic} / E' m_s$) parameter as a criterion to determine the nature of the deformation. The condition to determine the nature of the deformation is:[3]

$\gamma \leq 0.33$ asperities deform Plastically

$\gamma \geq 3$ asperities deform Elastically

2.4.3 Plastic Models

This section describes the models, which are based on the assumption that the deformation of asperities is plastic in nature.

Cooper, Mikic, Yovanovich

Cooper, Mikic and Yovanovich proposed a theory for thermal contact resistance based on the assumption that the distribution of surface heights is Gaussian. The numerical form of the theory is:[2, 5]

$$h_c = 1.45 \frac{m_s k_s}{\sigma} \left(\frac{P}{H_c} \right)^{0.985} \quad (11)$$

H_c is the micro hardness of the softer material at the interface. This theory was found to correlate well to experimental data.

Yovanovich

Yovanovich later modified equation (11) to: [2]

$$h_c = 1.25 \frac{m_s k_s}{\sigma} \left(\frac{P}{H_c} \right)^{0.95} \quad (12)$$

Equation (12) was found to correlate better to experimental data for a wider range of (P/H_c) values.

Mikic

Mikic also proposed a theory with the assumption of plastic deformation of the asperities, which can be formulated as: [2, 6]

$$h_c = 1.13 \frac{m_s k_s}{\sigma} \left(\frac{P}{H_c} \right)^{0.94} \quad (13)$$

It is observed that all the models differ only in terms of the constants used in the equations. These were varied from one model to another to obtain better correlation to the experimental data.

Further studies were carried out and it was concluded by Greenwood and Wu that the deformation tend to be plastic at light loads and become elastic at higher loads. [3, 4] In this study the components considered are under the influence of low loads and hence the plastic models discussed in this section will be used to determine the value of thermal contact resistance.

2.5 Treatment of oxidised surfaces

The thermal contact resistance of a material increases when the surface is oxidised. The oxide layer is generally harder than the parent material. Madhusudana states that the thermal contact resistance of an oxide layer is higher by one or two orders than the parent material. [7]

The presence of oxide layers can also disrupt the metal to metal contact and thereby increase the resistance to heat transfer. The oxide layers can also make the metal brittle and break up the metal-metal contacts. This also increases the surface roughness which, leads to an overall increase in the thermal contact resistance. [8]

The thickness of the oxide layer is generally small, so the effect of oxide layer on Thermal contact resistance is small for wavy and non-flat surfaces. However for flat surfaces the effect of oxide layers can be quite significant. A theory to calculate the thermal contact resistance for oxide layers was proposed in [7].

$$R_c = 66 P^{-0.945} \sigma^{-0.128} X^{0.0346} \quad (14)$$

Where X is the total film thickness of the oxide layers for each contact surfaces.

2.6 Treatment of welded surfaces

Understanding the joint topography is essential to predict the thermal contact resistance of a welded joint. The topography of individual joints can vary depending on the filler material and the quality of the welding process. The presence of voids in a welded joint can cause the thermal contact resistance to vary from one joint to another. The investigation of each individual joint through experiments or CFD simulations can be tedious and is not feasible. Therefore, a general theory which can predict the contact resistance for all joints with a small compromise on accuracy is the key to solving the problem.

The increase in the contact resistance at a joint, is due to the reduction in the contact area due to the presence of a void.

H. Zhao et al. proposed that the overall joint resistance can be expressed with the help of a resistance model as:[9]

$$\frac{1}{R_j} = \frac{1}{R_t} + \frac{1}{R_G} + \frac{1}{R_R} \quad (15)$$

Here R_j is the total joint resistance. R_t is the thermal contact resistance of the welded joint, which involves the resistance due to the change in contact area (spreading resistance) and the conductive resistance offered by the filler material. R_G and R_R are the resistance offered due to any trapped gas in the void and the radiative resistance respectively. Figure 2.5 shows the visualization of the resistance model at a welded joint.

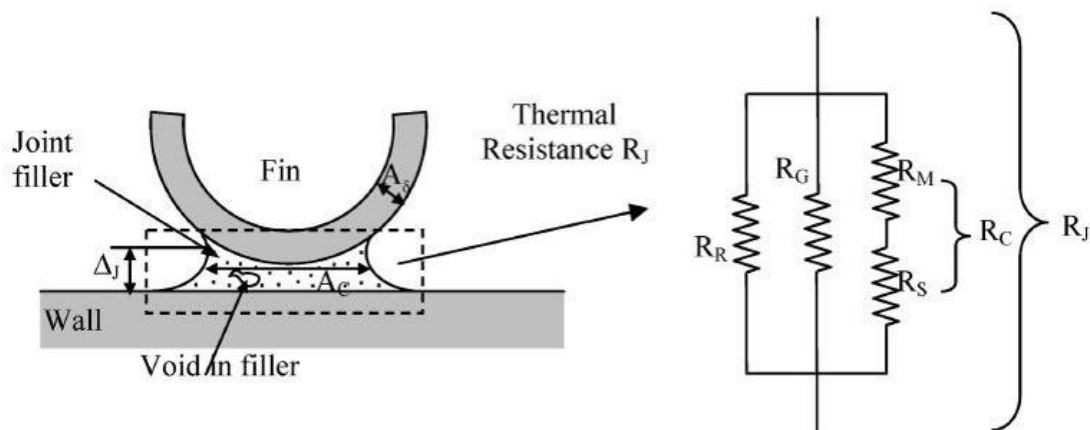


Figure 2.5 Visualisation of an imperfect welded joint and the resistance model

The spreading resistance is the biggest contributor to the joint resistance and it can be formulated as: [9]

$$R_s = A_s \frac{\Psi(\zeta)}{2ka} \quad (16)$$

$$\Psi = (1-1.4\zeta) \quad \text{if } \zeta < 0.5$$

$$\Psi = (1-\zeta)1.5 \quad \text{if } 0.5 \leq \zeta \leq 1$$

ζ is the square root of the ratio of the actual contact area to the real contact area. The model gives an approximation for estimating the contact resistance of the welded joints. [9]

The spreading resistance based on equation (16) was calculated, and the spreading resistance was found to be $8e-4 \text{ m}^2 \text{ K/W}$. The calculations were performed using a matlab script shown in Appendix A.

2.7 Parametric Study

A parametric study was carried out to estimate the material properties that affect thermal contact resistance for different materials. Table 2-1 shows the values obtained for the material properties from literature. [7, 10-13]

Table 2-1 Material properties for different materials

	Aluminum	Mild Steel	Stainless Steel
Thermal Conductivity (W/mK)	201.07	52.02	19.00
RMS Surface Roughness(μm)	0.12	0.12	0.41
Asperity Slope	0.03	0.03	0.14
Micro-hardness(MPa)	1400	2227	3800

	Rubber	Nylon	Polyethylene
Thermal Conductivity (W/mK)	0.15	0.29	0.39
RMS Surface Roughness(μm)	2.40	1.23	1.92
Asperity Slope	1.90	0.20	0.24
Micro-hardness(MPa)	560	410	410

3 Procedure

The method developed predicts thermal contact resistance by combining experiments and simulations in Radtherm™. In this section the methodology of the experiments and simulations are presented. Also, the criteria for selection of components to be tested is described in this section.

3.1 Sensitivity Analysis

The first part of the study was to determine which components are affected by thermal contact resistance. A sensitivity analysis was performed to identify these components.

The analysis was performed in Radtherm™. The thermal model of the engine bay and exhaust system was used and the thermal contact resistance was increased and decreased from the default value in steps by a factor of 10.

The components which showed large differences in surface temperatures as compared to the default case were identified as critical components to perform further analysis.

Figure 3.1 shows the temperature difference of a component.

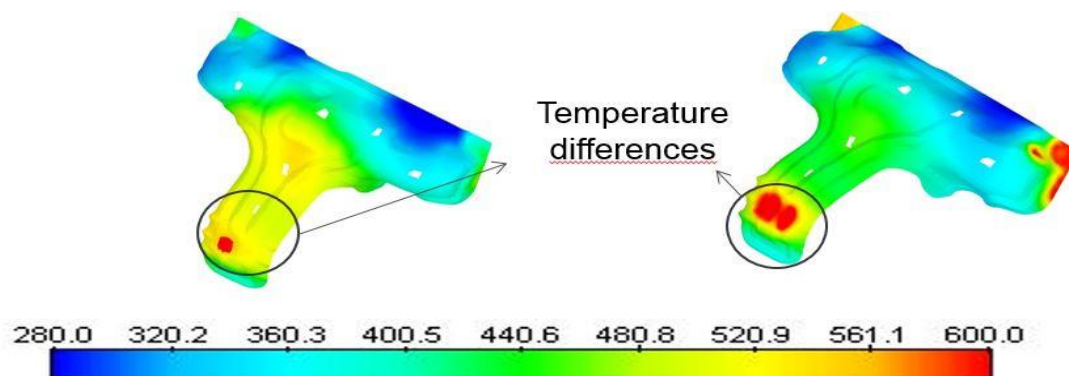


Figure 3.1 – Example case for sensitivity analysis

3.2 Experimental Setup

Experiments were designed to study individually, the heat transfer mechanism in several components. In order to increase the accuracy of the results obtained, it was essential to control the boundary conditions of the experiments.

As discussed in section 2.2, contact resistance is purely governed by thermal conduction. Hence the effect of convection and radiation had to be minimised to isolate the effect of conductive heat transfer within the component. To achieve this, the component was insulated using glass fibre insulation to prevent the heat loss to the surroundings due to convection.

The insulated component was clamped to a low conductive surface to decrease heat transfer to the clamping surface. The component was then heated using a heat gun at a small location which was left uncovered. The temperatures at different locations on the components were then recorded using thermocouples, which was connected to a CAN system. The thermocouples were either welded or glued on to the component depending on the material under consideration. Also, the position of the thermocouples were measured to decrease the uncertainty when comparing experimental results with simulations.

The components were heated until the temperatures on all the thermocouples reached a steady state value. The recording continued until the component reached room temperature again. In this way an entire cycle of heating and cooling was recorded while performing the analysis.

Figure 3.2 shows the placement of the thermocouples can be observed.



Figure 3.2 Experimental Setup and Placement of Thermocouples

Figure 3.3 shows the component after it was insulated.

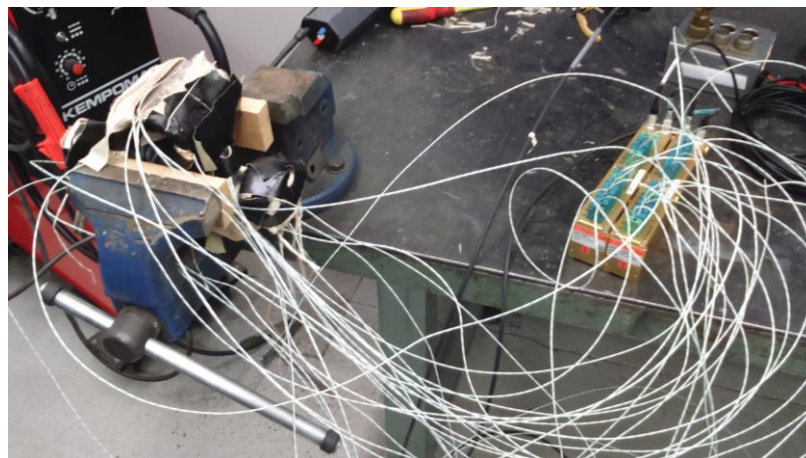


Figure 3.3 Experimental setup after insulation of the component

3.3 Simulation Setup

The results from experiments were compared with results from the simulation. The boundary conditions produced in the experiments was recreated in the simulations to obtain a valid comparison between the two methods. The setup of the simulations is divided into following steps:

3.3.1 CAD Cleaning

Usually the geometry from the design phase has a few double faces and intersections, which can cause the results to be unreliable. To avoid this problem, the geometry was cleaned before being imported into a thermal or CFD solver. The CAD cleaning was performed in Ansa. The heated portions were assigned a new PID (Part ID), to be able to assign different boundary conditions to them.

3.3.2 Meshing of the thermal model

The mesh generated for the component is crucial to ensure that reliable solutions are obtained. The surface meshing was also done in Ansa. The type of mesh generated depended on the material of the component under consideration. Metal components have good thermal conductivity and hence a 2D surface mesh was generated for the simulations. But components made of rubber or plastic have lower thermal conductivity and so a 3D volume mesh was generated to better capture the thermal conductance through the material.

Once the mesh was generated the quality had to be checked to ensure that all the elements were within the quality limits specified to avoid divergence of the solution. Also, it has to be mentioned that this mesh generated was for the thermal simulation. Table 3-1 shows the quality criterion for the mesh which was generated.

Table 3-1 Quality criterion for Mesh

Parameter	Value
Aspect Ratio	3
Skewness	0.5
Warping	40
Mesh Distortion	1
Max Angle Quads	0.7
Max Angle Trias	0.7

The problematic areas were then corrected by reconstructing the mesh in these areas or by reshaping them. Quad elements were used for 2D meshing and Hex Poly elements were using for generating the volume mesh. These elements were chosen since having elements with more edges, captures the heat transfer in a more accurate way.

3.3.3 Thermal Model Setup

The geometry and the mesh were output from Ansa and imported into Radtherm to perform the thermal analysis. The material properties were then assigned to the components.

The aim of the thermal simulations was to reproduce the same conditions as in the experiments at the heated surfaces. This means that the initial conditions for the simulations, such as the surface temperatures at the portion which was heated remained the same as recorded in the experiments. Thermal contact resistance of the materials were then varied, to get the same temperature distribution as observed in the experiments at all measurement points on the component. This value of contact resistance was then compared with the values obtained in the parametric study to ensure that the value calculated was physically correct. The simulations were also performed using the default values of thermal contact resistance to evaluate its influence.

For some components the boundary conditions were very hard to control in experiments and hence it was not possible to attain a steady state solution. Therefore, a transient analysis was performed on these components and the temperature distribution was studied at different time instances.

The differences in the temperatures observed between the experiments and the simulations were recorded and plotted.

3.4 Coupling Thermal Simulations with a CFD Software

In order to have a closer resemblance to the real conditions, a CFD software was coupled to the thermal model of the complete engine bay and exhaust system. The CFD software resolves the heat transfer co-efficients and the air film temperatures around the components. The Radtherm model provides the temperature profile, by considering the conductive and radiative heat transfer.

The process was carried out using an automated script developed at VCC. First the thermal model is run using an initial guess for the heat transfer co-efficient and the local air temperatures. The output is a temperature profile which is then input into Fluent. Using this initial temperature profile, Fluent solves the heat transfer co-efficient and air temperatures, which are again used as inputs by Radtherm. This loop was repeated 5 times to ensure that a converged solution was obtained. Figure 3.4 shows the schematic of the coupling process.

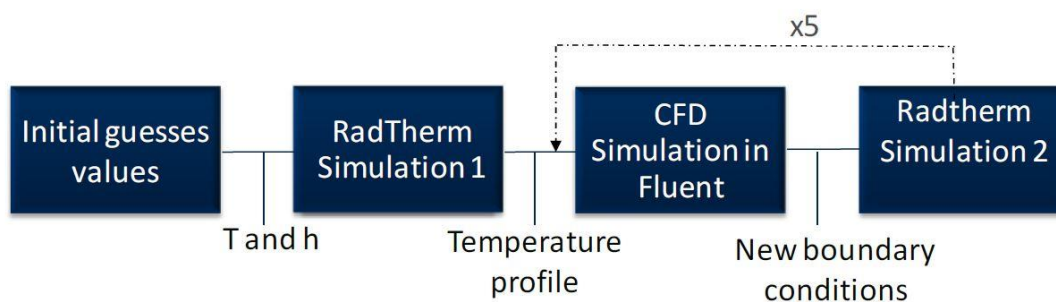


Figure 3.4 Schematic of the coupling process [14]

4 Results and Discussion

This section presents the results from the parametric study and the sensitivity analysis. This will be followed by the results from the component level tests and the full vehicle simulations.

4.1 Results from the Parametric Study

The parametric study was carried out to estimate the material properties that affect contact resistance. Based on the material properties in Table 2-1, the thermal contact resistance was calculated using equation (13). The Mikic model was used to calculate the values of contact resistance, because it accounts for the elastic deformation around the plastic flow of the micro asperities. [2] Also, it was found to correlate better to the data obtained from experiments. The thermal contact resistance was calculated for different values of contact pressure, to obtain a range in which the parameter can vary for different combination of materials. The value was calculated for most of the material combinations found in the engine bay and exhaust system.

The calculations were performed using a matlab script as shown in Appendix B. Table 4-1 shows the values for contact resistance. The range specified is for different values of contact pressure.

Table 4-1 Thermal Contact Resistance values for different combination of materials

Surface 1	Surface 2	Contact Resistance x 10 ⁻⁴ (m ² K/ W)
Mild Steel	Aluminum	0. 4-3
	Mild Steel	0. 9-8
	Rubber	13-120
	Stainless Steel	10-11
	Polyethylene	25-220
Stainless Steel	Aluminum	0. 6-5
	Rubber	14-120
	Polyethylene	22-200
	Stainless Steel	3.7-26
Aluminum	Aluminum	0.16-1.4
	Rubber	13-110
	Nylon	25-220
	Polyethylene	25-220
Rubber	Nylon	18-158
	Polyethylene	18-158
	Rubber	27-239
Nylon	Nylon	54-470
	Polyethylene	54-470
Polyethylene	Polyethylene	51-446

*Table Shows values of Thermal Contact Resistance for pressure range 0.1 – 1 MPa
It can be seen that materials with a low value of thermal conductivity have higher values of thermal contact resistance.

4.2 Results from the Sensitivity Analysis

The sensitivity analysis was carried out to determine the list of components that have to be analysed. Based on the the results of the sensitivity analysis four components were selected:

- Downpipe and Exhaust Hangers
- Powertrain Mount
- Manifold Heat Shield
- Cam Belt Cover

Figure 4.1 shows the four components.

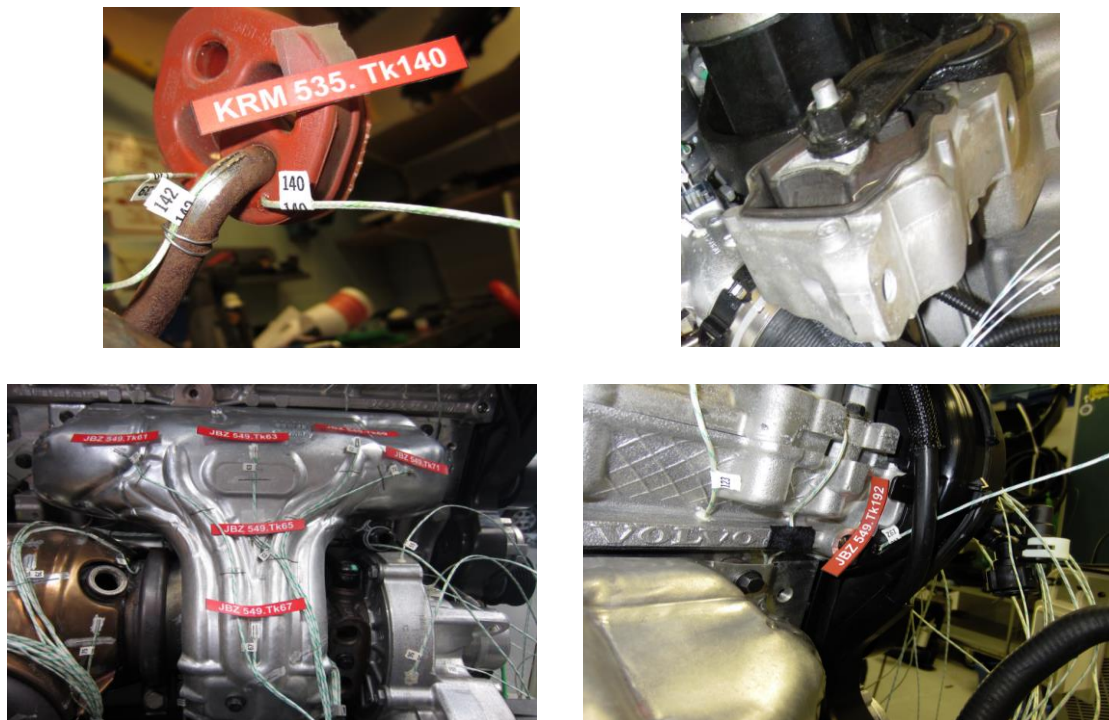


Figure 4.1 – Components to be studied in the thesis

The Figure 3.1 shows the results of the sensitivity analysis which was performed on the manifold heat shield. The temperature difference due to the change in the value of the contact resistance can be seen in that figure. This was used as a criterion to determine which components needed further analysis.

4.3 Component Analysis

This section contains the results from the component level analysis.

4.3.1 Downpipe and Exhaust Hanger

The analysis of the downpipe and exhaust hanger had to be carried out in two phases. One phase was to study the heat transfer across the welded joint, and the other phase was to study the interface between the steel pipe and the rubber hanger.

Welded Joint Interface

Figure 4.2 shows the highlighted surface that was heated in the experiment. Also, in the simulations thermal links were used to specify the value of contact resistance across different interfaces.

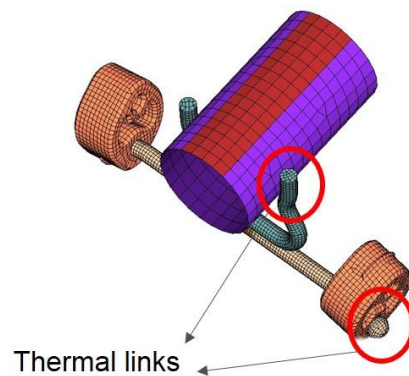


Figure 4.2 Model Setup for experiments and Simulation for the downpipe

Figure 4.3 shows the location of the thermocouples on the component.

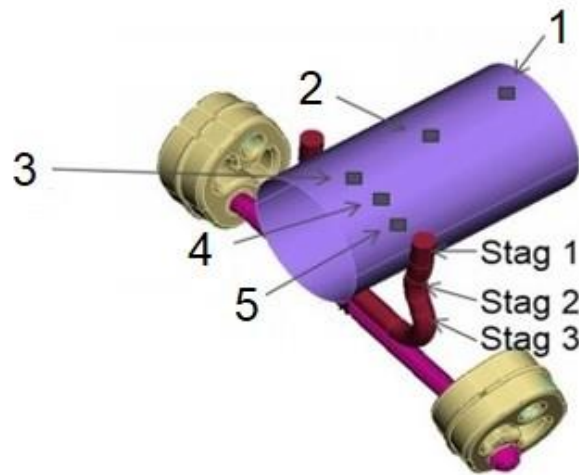


Figure 4.3 Nomenclature of thermocouples fo downpipe

The simulations were carried out with two values of contact resistance and the temperatures at the measuring points were compared with those from the tests. The difference between the temperatures observed in the experiments and the temperatures from the simulations, were plotted for both cases at each measurement point. The same case was also repeated for two values of emissivities of steel.

$$\Delta T = (\text{Temperature of thermocouple from the experiment}) - (\text{Temperature of thermocouple from the simulation})$$

Figure 4.4 shows the comparison of ΔT for both the values of contact resistance and a emissivity of 0.5. The absolute values of the temperatures at these thermocouples can be seen in Appendix C.

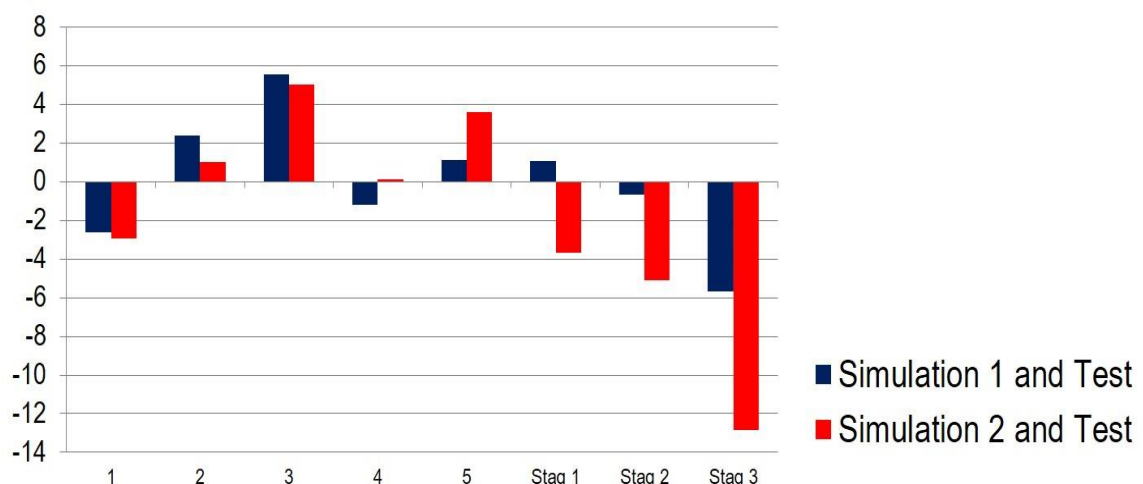


Figure 4.4 ΔT values for emissivity of 0.5 for two contact resistance values.

Simulation 1 : $R_c = 7e-4 \text{ m}^2 \text{ K/W}$ Simulation 2 : $R_c = 1e-4 \text{ m}^2 \text{ K/W}$

Figure 4.5 shows the results for the case with the emissivity of 0.7.

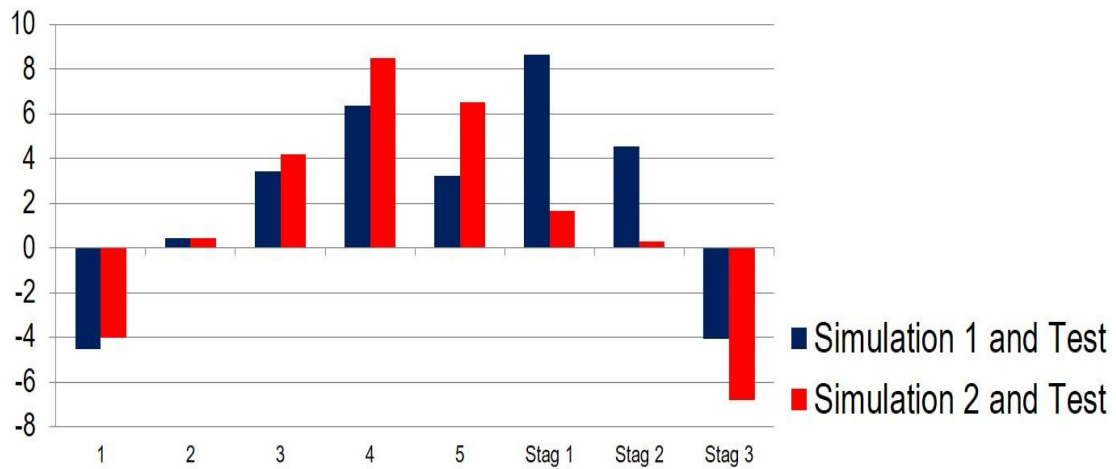


Figure 4.5 ΔT values for emissivity of 0.7 for two contact resistance values.

Simulation 1 : $R_c = 7e-4 \text{ m}^2 \text{ K/W}$ Simulation 2 : $R_c = 1e-4 \text{ m}^2 \text{ K/W}$

Figure 4.6 shows the temperature distribution on the surface of the downpipe and the stag.

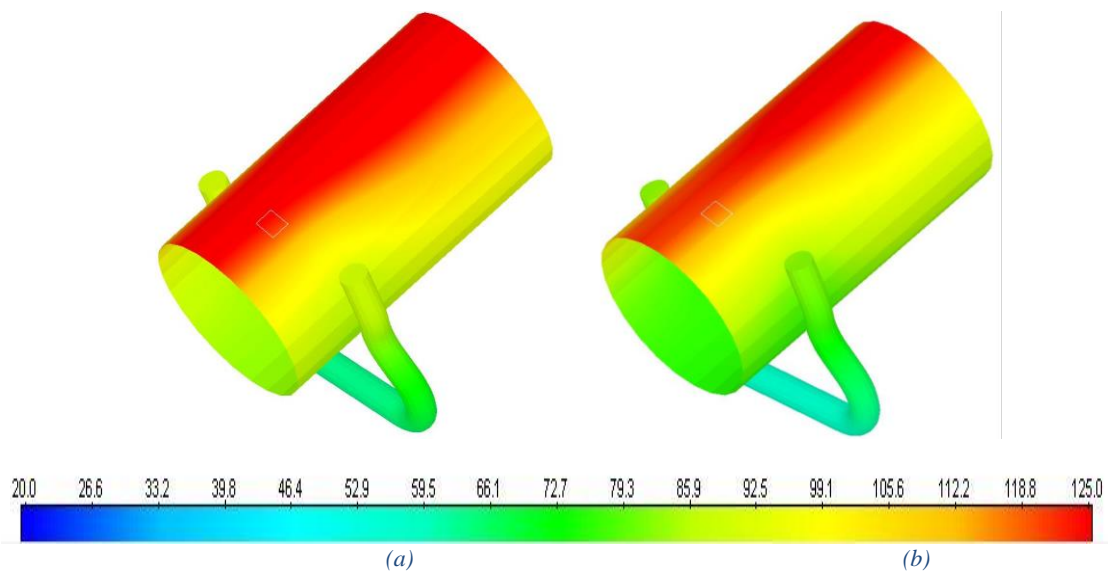


Figure 4.6 Temperature distribution on the downpipe

a) Emissivity = 0.5 b) Emissivity = 0.7

It can be observed that the surface temperatures decrease as the value of emissivity is increased. The material tends to lose more heat through radiation as the emissivity is increased. The contact resistance value of $7e-4 \text{ m}^2 \text{ K/W}$ was found to correlate better to the experimental results as compared to the default value of $1e-4 \text{ m}^2 \text{ K/W}$. This value was found to lie in the range of contact resistance which was calculated in table 4.1.

The best fit values for the emissivity and contact resistance were 0.5 and $7e-4 \text{ m}^2 \text{ K/W}$ respectively for this configuration.

Figure 4.4 shows high deviations between the experimental and simulation results for the measurement point 'stag 3'. This can be attributed to the losses due to convection to the surroundings. Due to the curved shape of the component, it could not be insulated properly. But, these losses are not accounted for in the simulations and therefore bigger deviations were observed at this point. The small deviations at the other points can be attributed to the errors in the measurement techniques and also the error of the thermocouple itself. The thermocouples used were the uncalibrated k-type thermocouples. They have an error of $\pm 2.1 \text{ }^\circ\text{C}$ for the temperature range $-40 \text{ }^\circ\text{C}$ to $375 \text{ }^\circ\text{C}$ and $\pm 6.5 \text{ }^\circ\text{C}$ in the range of $375 \text{ }^\circ\text{C}$ to $1000 \text{ }^\circ\text{C}$. [14]

Steel Rubber Interface

The second phase was to study the interface between the steel pipe and the rubber hanger. Figure 4.7 shows the heated portion for the stag and rubber interface.

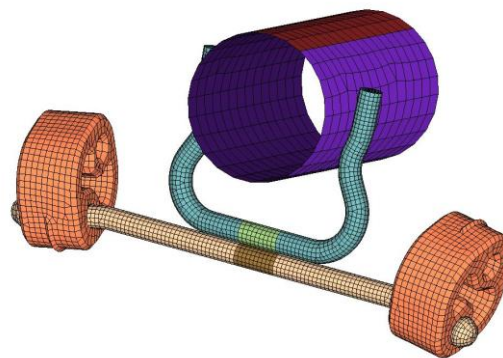


Figure 4.7 Visualisation of the heated portion of the stag

Figure 4.8 shows the nomenclature of the thermocouples on the exhaust hanger.

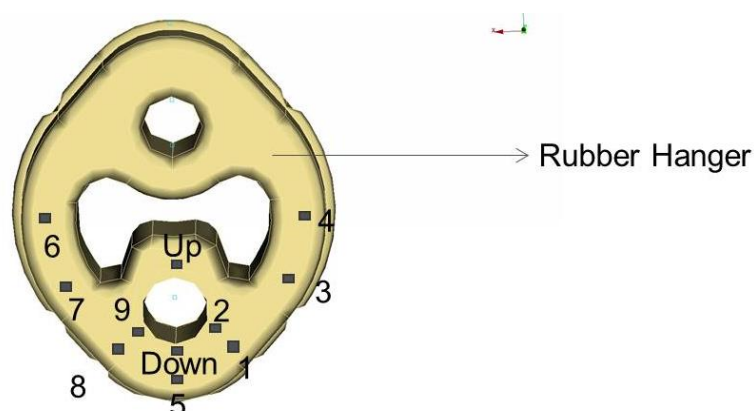


Figure 4.8 Nomenclature of the thermocouples on the rubber hanger

As mentioned in the previous section the same procedure was adopted and the difference in temperatures between the experiments and simulations were recorded. Here the contact resistance value of $0.012 \text{ m}^2 \text{ K/ W}$ and the default value of $0.021 \text{ m}^2 \text{ K/ W}$ were used and compared. The simulation was also carried out for the

emissivity values of 0.5 and 0.7 for steel. The values were recorded for the outer surface of the rubber stag.

Figure 4.9 and Figure 4.10 shows the ΔT values for all cases. The absolute values of the temperatures at these thermocouples can be seen in Appendix C.

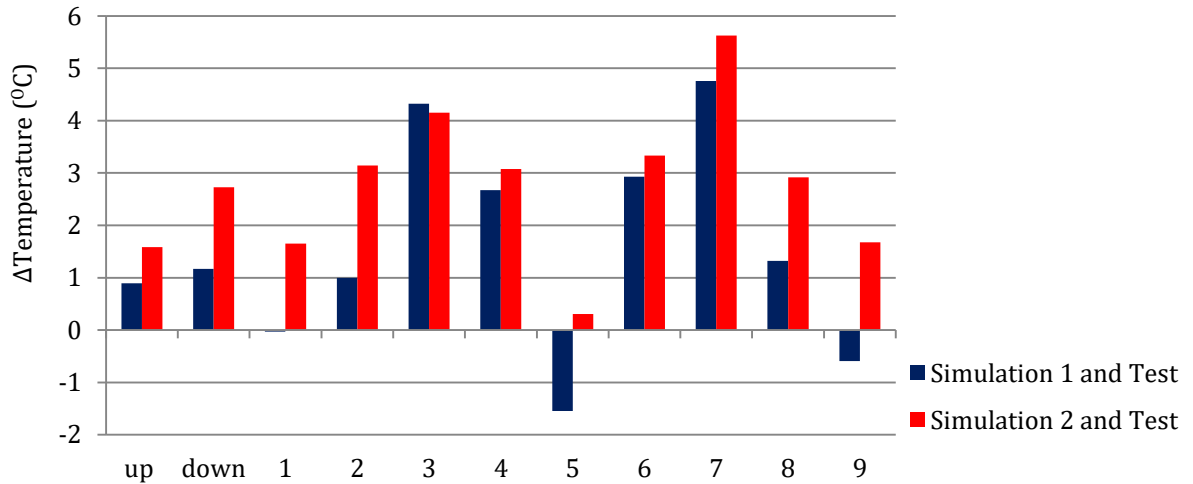


Figure 4.9 ΔT values for emissivity of 0.5 for two contact resistance values.

Simulation 1 : $R_c = 0.012 \text{ m}^2 \text{ K/W}$

Simulation 2 : $R_c = 0.021 \text{ m}^2 \text{ K/W}$

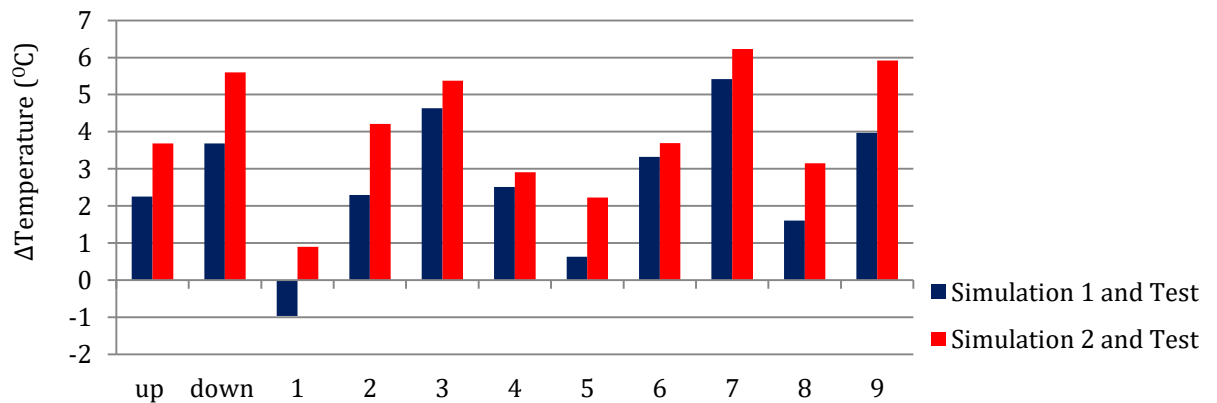


Figure 4.10 ΔT values for emissivity of 0.7 for two contact resistance values.

Simulation 1 : $R_c = 0.012 \text{ m}^2 \text{ K/W}$

Simulation 2 : $R_c = 0.021 \text{ m}^2 \text{ K/W}$

It can be seen that the contact resistance value of $0.012 \text{ m}^2 \text{ K/W}$ and emissivity value of 0.5 gave the best correlation to the data from experiments.

Figure 4.11 shows the temperature distribution on the exhaust rubber.

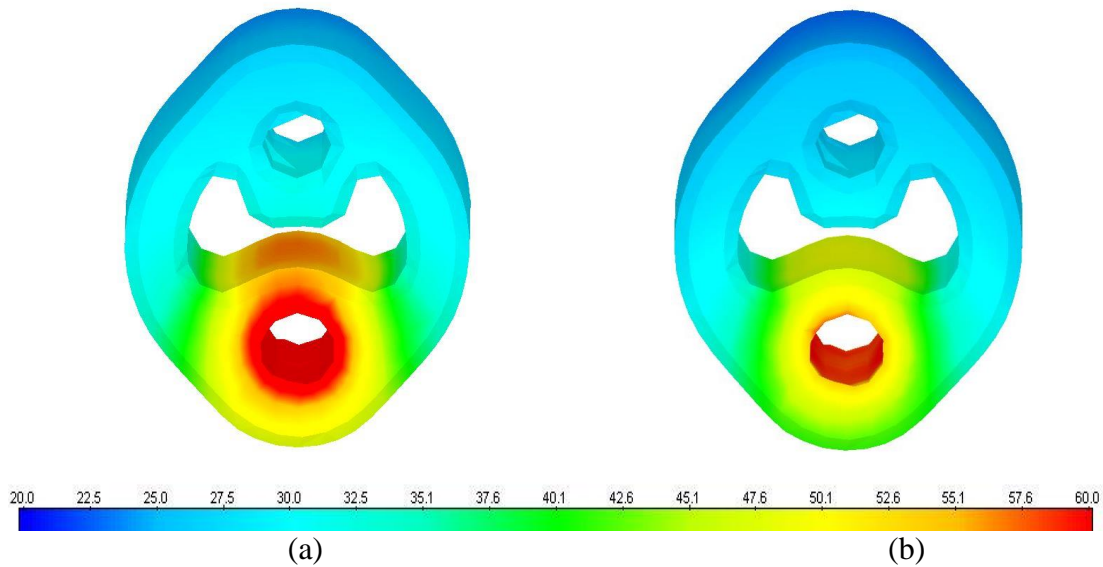


Figure 4.11 Temperature distribution over the rubber hanger

(a) Emissivity = 0.5 (b) Emissivity = 0.7

It can be noticed that the thermocouples close to the stag are affected more by thermal conduction. This causes the temperature of these thermocouples to be lower as the stag itself presents a lower temperature. This was observed for both the outer and the inner surface of the rubber hanger. The thermocouples further away from the stag were not affected considerably due to the change in emissivity. The outer surface is not exposed to the steel pipe and is consequently not considerably affected by radiation. Whereas the inner surface of the rubber hanger which is facing the steel pipe is exposed more to the radiation from the steel pipe. Therefore, a slightly higher temperature was observed at the thermocouples further away from the steel pipe for the inner surface.

Also, the deviation in ΔT values at points 3 and 7 are high, when compared to the other measurement points. This can be explained by improper insulation at those points, as these points are located at the curvature of the rubber hanger. Also, the uncertainty of the thermocouple position, especially in the areas of high temperature gradients can cause the results to vary from the experiments and simulations. Being a component with low thermal conductivity, the temperatures recorded are sensitive to the point of measurement.

4.3.2 Manifold Heat Shield

The manifold heat shield is a multi layer component. It consists of an insulation layer sandwiched between two layers of metal. The aim was to determine the resistance offered by the layer of insulation to the heat transfer. This resistance to the heat transfer is a summation of the resistance due to the contact resistance at the two interfaces between the metal and insulation and also due to the low thermal conductivity of the insulation. It is very complicated to isolate the individual effects of these resistances and therefore the combined effect is estimated in this thesis.

A small portion of the heat shield was considered for the analysis. The top and the bottom layers of the heat shield were in contact with each other at the edges. The metallic contact had to be cut off to ensure that there was no conduction of heat around the insulation and to the bottom layer. This ensured that the heat transfer through conduction between the two metal layers could only take place normally through the insulation.

Figure 4.12 shows the portion of the heat shield which was heated and the nomenclature of the thermocouples.

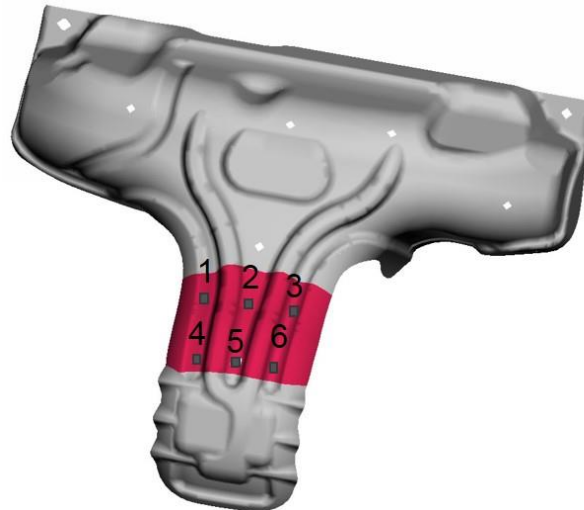


Figure 4.12 Visualisation of the heated poortion of the heat shield and Nomenclature of thermocouples

Figure 4.13 shows the experimental setup for the heat shield.



Figure 4.13 Experimental setup for the heat shield experiment

As mentioned in section 3.3.3 a steady state temperature was difficult to achieve on the heat shield. Therefore, a transient analysis had to be performed on the heat shield to compare the results of the simulation with experiments. In the experiments the top layer of the heat shield was insulated and the bottom layer was heated. The bottom layer was heated for 5 minutes and then allowed to cool down. The temperature distribution was

compared at two different time instances of 7 minutes and 8 minutes to ascertain the accuracy of the solution.

Figure 4.14 and Figure 4.15 show the temperature distribution over the surface at two different time intervals for the portion of the heat shield under consideration.

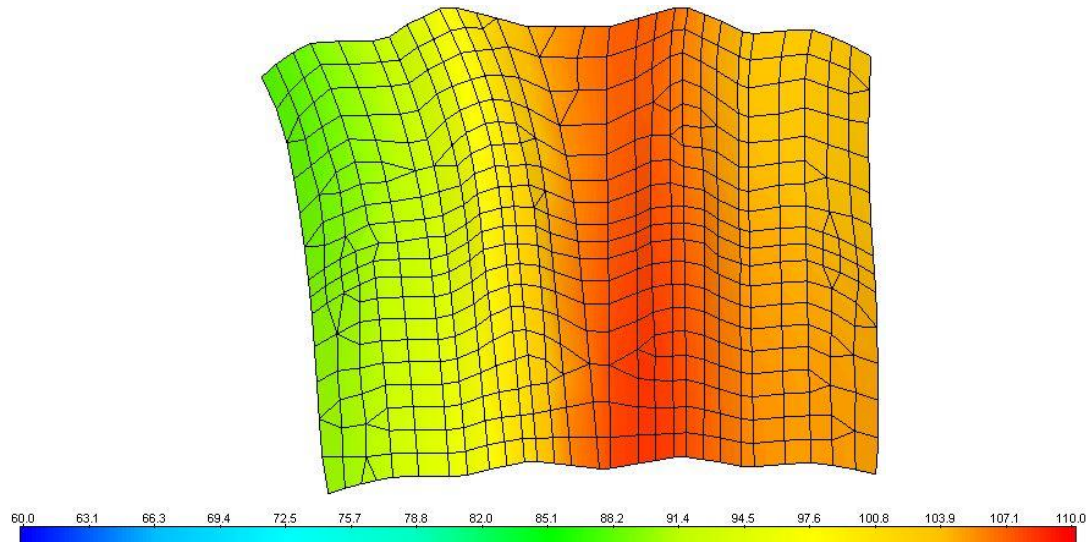


Figure 4.14 Temperature distribution over the heat shield after 7 minutes

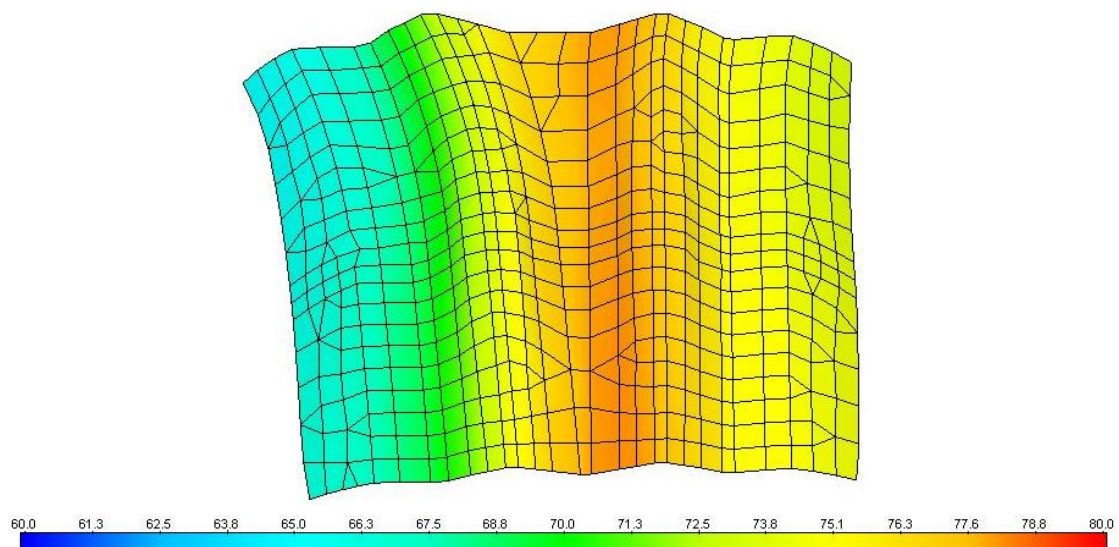


Figure 4.15 Temperature distribution over the heat shield after 8 minutes

$\Delta T = (\text{Temperature at the top layer of the heat shield}) - (\text{Temperature at the bottom layer of the heat shield})$

Figure 4.16 and Figure 4.17 show the ΔT values at all the measurement points from the experiment and the simulation. The absolute values of the temperatures at these thermocouples can be seen in Appendix D.

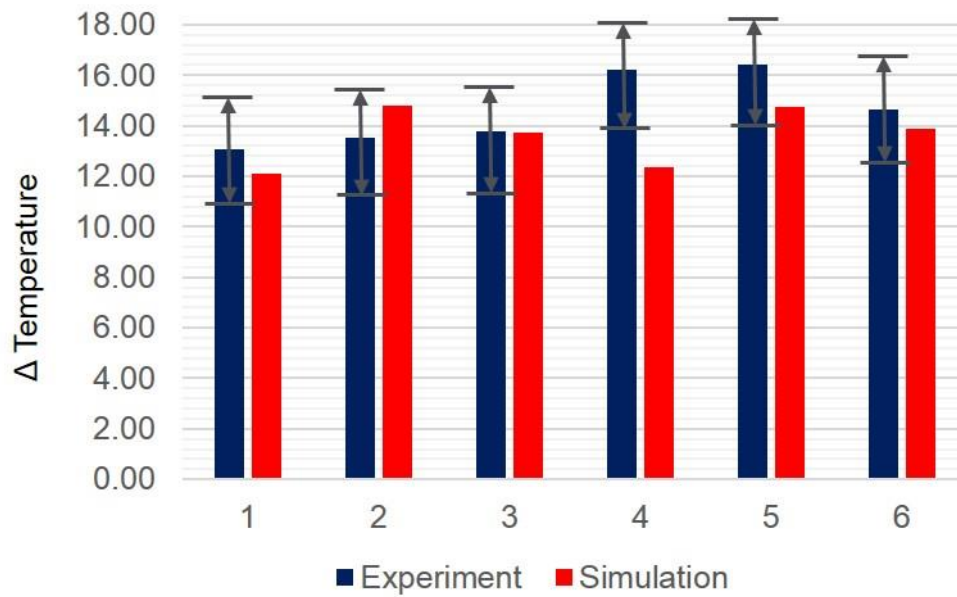


Figure 4.16 Delta T between the top and the bottom layers after 7 minutes

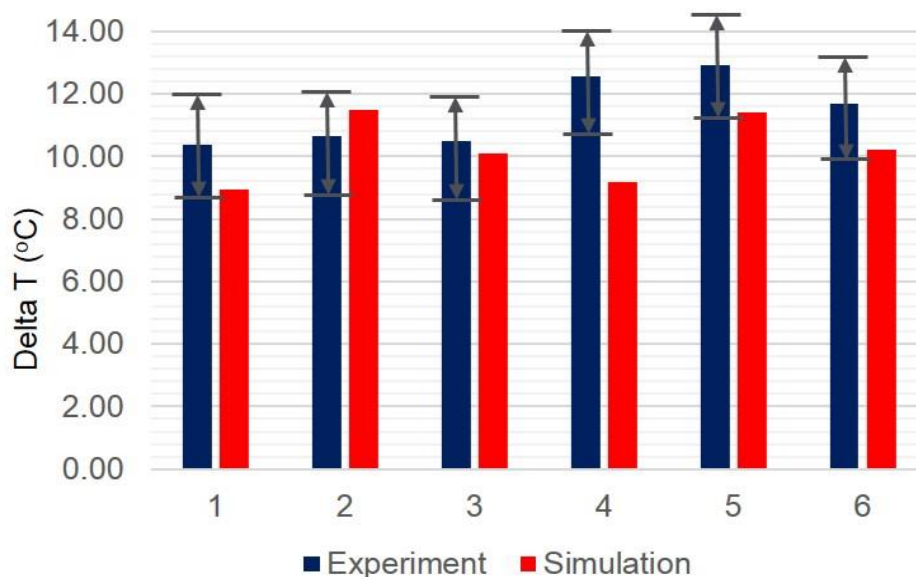


Figure 4.17 Delta T between the top and the bottom layers after 8 minutes

It can be observed that for all the points the ΔT values from the experiment and the simulation correlate with each other. The small deviations can be explained due to errors in measurement from the thermocouples and small effects of convective heat losses in experiments which are not encountered in the simulations. It was also observed that the ΔT changes when the surface temperatures changes in the two time intervals. This can possibly be attributed to the change in radiative heat losses that occur when the temperature changes.

At point 4, a higher ΔT value was observed in the experiments. This was possibly due to an error encountered in the experiment. In the original component the layers were pressed together. As the edges were cut off, the layers of the heat shield were prone to separating from each other. The layers of the heat shield were hence held together using plastic cable ties. Plastic was used to prevent any heat transfer through them. Upon heating the heat shield the plastic cable tie melted which led to an increase in the gap

between the two metal layers. This could have caused the conductivity to reduce and thereby leads to a larger temperature drop across the insulation.

The conductivity of 0.07 W/m K for the insulation gave results which correlated to the tests. When the simulations were performed with the default value of 0.1 W/m K, the ΔT s were found to increase by 3-4 degrees. This value of conductivity of 0.07 W/m K, gave the thermal resistance of the insulation as 0.014-0.021 m² K/W depending on its thickness.

4.3.3 Powertrain Mounts

The interface between aluminum and rubber was studied in this component. Figure 4.18 shows the experimental setup for the powertrain mount.



Figure 4.18 Experimental setup for the powertrain mount

Figure 4.19 shows the nomenclature of the thermocouples. The heated portion can also be seen in the figure. The contacts 3 and 4 were located on the opposite side of 1 and 2 respectively.

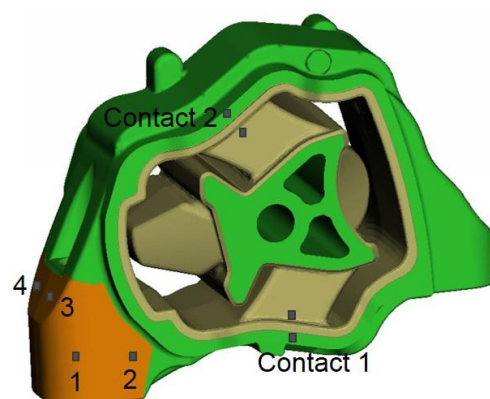


Figure 4.19 Nomenclature of thermocouples for the powertrain mounts

The temperature drop across the interface at four different locations was estimated and the values from experiment were compared to the values from simulation.

$$\Delta T = (\text{Temperature of aluminium at interface}) - (\text{Temperature of rubber at the interface})$$

The ΔT values were calculated for two values of contact resistance. The values used were $0.011 \text{ m}^2 \text{ K/W}$ and the default value of $0.021 \text{ m}^2 \text{ K/W}$. Figure 4.20 shows the results for both the cases. The absolute values of the temperatures at these thermocouples can be seen in Appendix E.

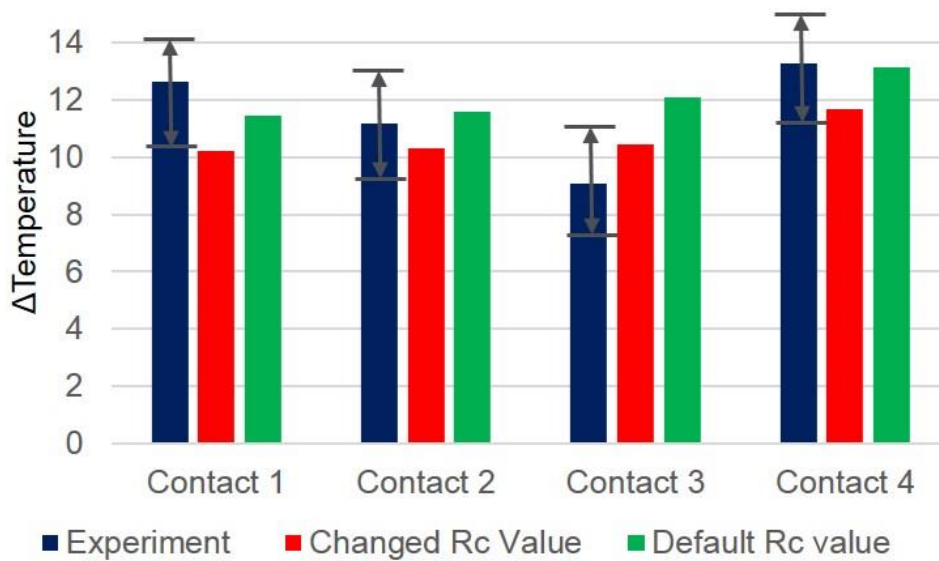


Figure 4.20 Drop in temperature across the aluminum rubber contact

Changed R_c value = $0.011 \text{ m}^2 \text{ K/W}$

Default R_c Value = $0.021 \text{ m}^2 \text{ K/W}$

Figure 4.21 shows the surface temperature distribution on the powertrain mounts.

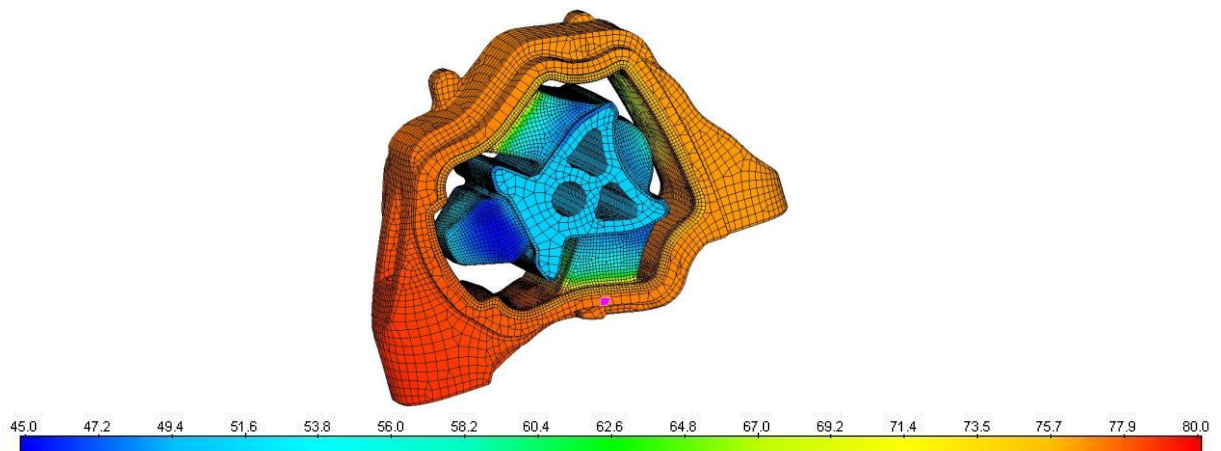


Figure 4.21 Temperature distribution over the surface of the powertrain mount

It was observed that the default value of $0.021 \text{ m}^2 \text{ K/W}$, gave better correlation to the experimental results. Although, it has to be mentioned that the difference between the experimental results and the simulation results for both cases lie within the range of uncertainty of measurement for the thermocouples. A more detailed analysis of the material properties will have to be carried out to determine the accurate value of contact resistance for this case. It can also be observed that the points further away from the heat source (interface 4) shows a higher value of ΔT . The thermocouples close to the heated portion can get heated directly by heat transfer through convection through gaps in the insulation. But this phenomenon is minimised for thermocouples further away, which can lead to slightly higher temperature drop across the interface.

4.3.4 Full Vehicle Simulation

The full vehicle simulation was carried out by coupling the thermal simulations to the CFD code. The coupling process was described in section 3.4. The full vehicle simulation was run by changing the value of contact resistance based on the values from Table 4-1 for all the contacts in the engine bay and the coupling simulation was executed. The results from the simulation were compared to the values from the simulation with the default values of contact resistance to study how the parameter effects the surface temperatures of the components in the engine bay and exhaust system.

Figure 4.22 shows the components whose temperatures were studied and also the their location in the engine bay and the exhaust system.

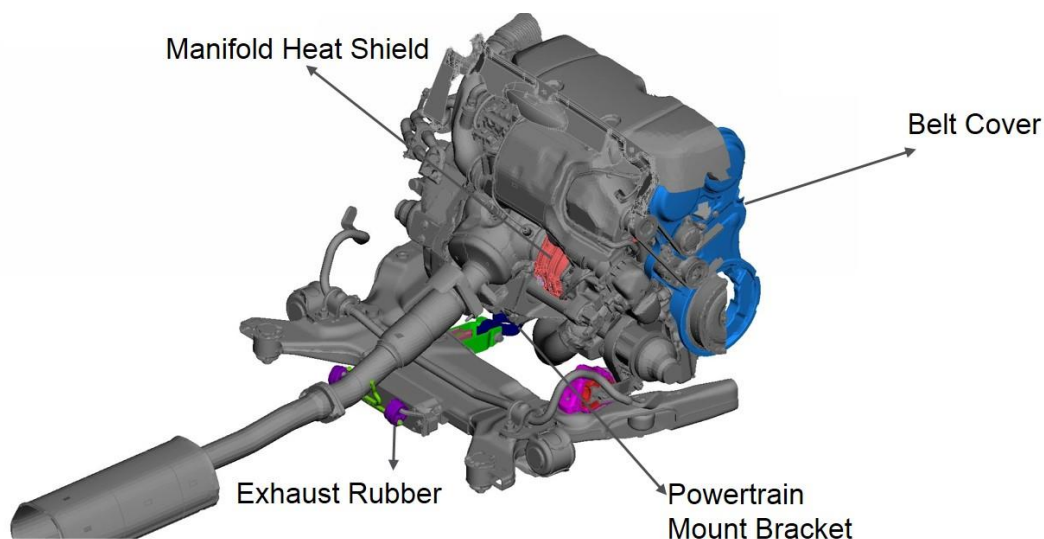


Figure 4.22 Location of different components in the engine bay and exhaust system

Belt Cover

The belt cover is the plastic, covering the cam belt in the engine bay. In the default case the belt cover was wrapped together with the engine block and the cylinder which caused the temperatures on the belt cover to be over estimated. In the changed simulation it was split from the engine cylinder and a contact resistance of $0.02 \text{ m}^2 \text{ K/W}$ was used for the simulations.

Figure 4.23 shows the location of the thermocouple on the belt cover at which the temperatures were measured.

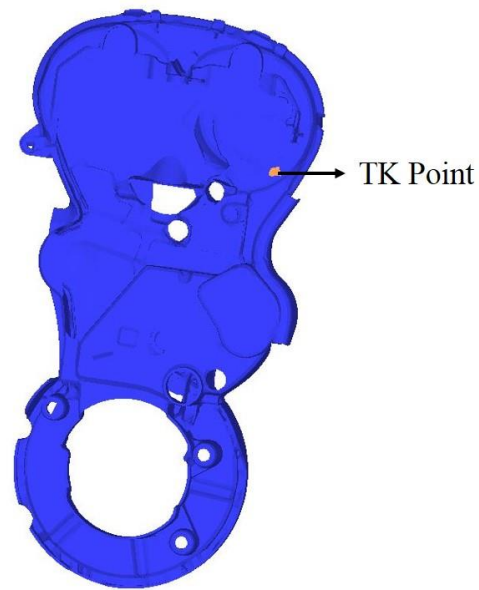


Figure 4.23 Belt cover with location of thermocouple

Manifold Heat shield

The results obtained in section 4.3.2 were used and the conductivity of the insulation was changed to 0.07 W/m K , to study its effect on the temperatures at various locations on the heat shield. Figure 4.24 shows the locations of the thermocouples.

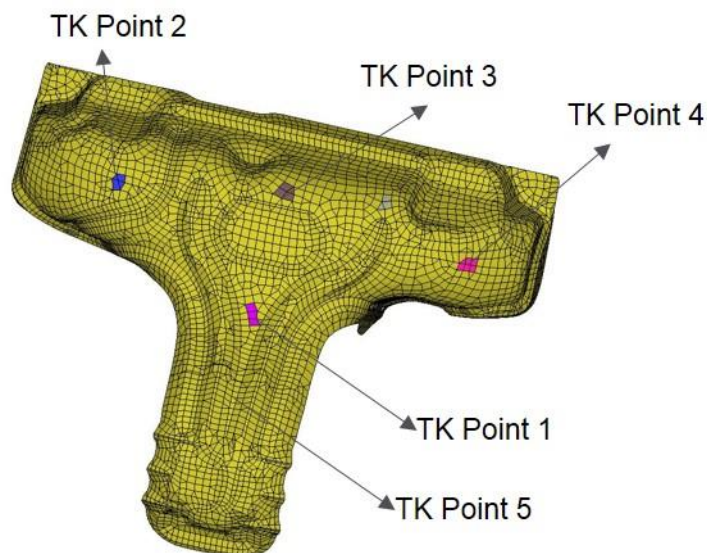


Figure 4.24 Location of thermocouples in the full vehicle simulations

Powertrain Mount Bracket

The temperatures at two different locations on the powertrain mount bracket was recorded. The default value of contact resistance was $0.021 \text{ m}^2 \text{ K/W}$, and the changed value was $0.012 \text{ m}^2 \text{ K/W}$. Figure 4.25 shows the location of the thermocouples on the component.

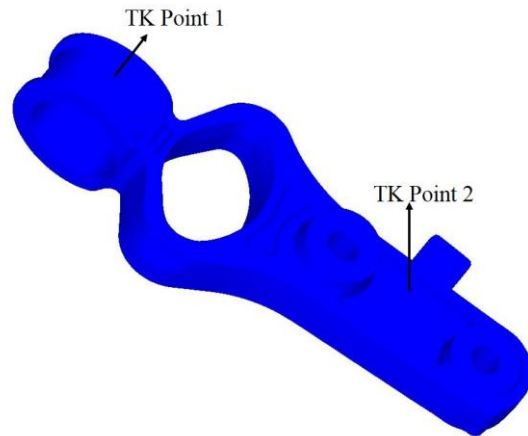


Figure 4.25 Nomenclature of the thermocouples for the powertrain mount bracket for the full vehicle simulation

Exhaust Rubber

The temperatures at two different locations on the exhaust rubber was recorded. The default value of contact resistance was $0.021 \text{ m}^2 \text{ K/W}$, and the changed value was $0.012 \text{ m}^2 \text{ K/W}$. Figure 4.26 shows the location of the thermocouples on the component.

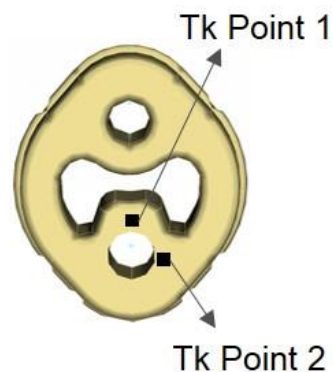


Figure 4.26 Nomenclature of the thermocouples for the exhaust rubber for the full vehicle simulation

Figure 4.27 shows the difference in temperature, observed at different locations between the default values and the changed values of contact resistance for all the components listed above.

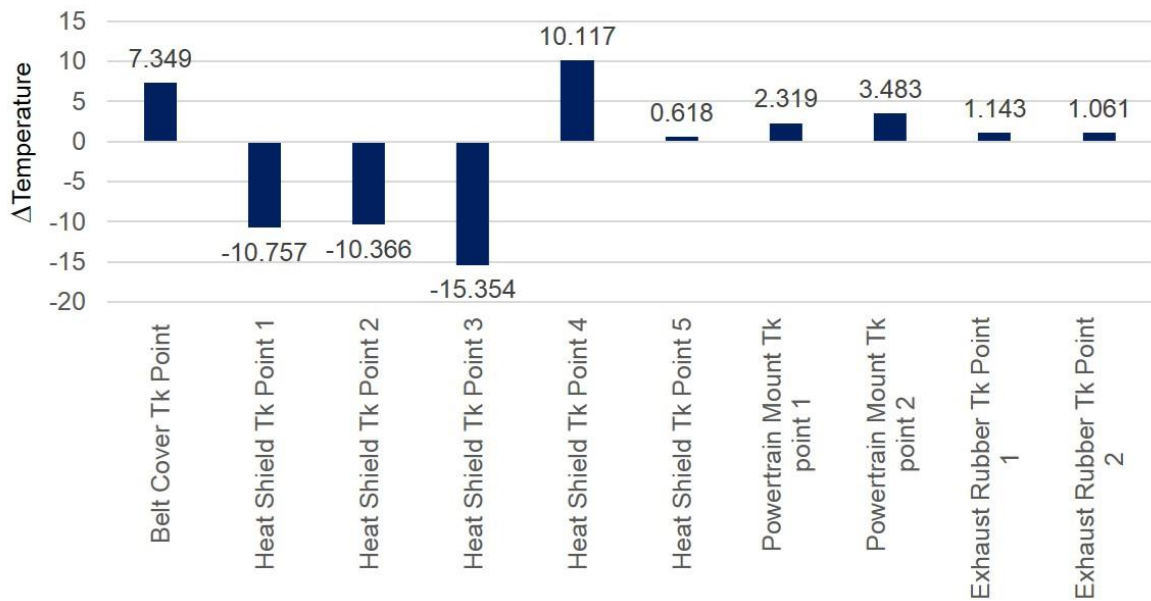


Figure 4.27 ΔT between default and changed value of R_c

These results from the full vehicle simulation were found to correlate better to the data from the wind tunnel, which was carried out earlier for the same driving cycle conditions.

It was also observed that the components which have low thermal conductivity were affected more by the value of thermal contact resistance. Other components in the engine bay showed deviation of around 1-2 degrees from the case using the default values of thermal contact resistance.

5 Conclusion and Scope for Future Work

A method to estimate the thermal contact resistance was developed, based on different material properties. Regardless of the assumptions made for the material properties the estimated values of contact resistance correlated to the experimental data for most components. Also, by using the values obtained from the method in the full vehicle simulations, a better correlation to the wind tunnel data was shown.

It was possible to control the boundary conditions in the experiments and reproduce them in simulations to compare the results. The thesis was helpful to understand the different modes of heat transfer and their effects on the temperatures of the components. Moreover, it was a good opportunity to learn about the different parameters that affect the surface temperatures of the components in the engine bay and exhaust system of vehicles.

The study was instrumental to identify the critical components that are affected by thermal contact resistance. They were found to be:

- Cam Belt Cover
- Manifold Heat Shield
- Powertrain Mounts
- Downpipe and Exhaust Hangers

The thesis also provided some details on the coupling process between thermal and CFD simulations.

In conclusion, the thesis was able to provide some inputs to the process of decreasing physical tests in the future and thereby reducing time and cost. The method developed can be used in future simulations to predict the heat transfer more accurately.

As a step to increase the accuracy of the predicted values of thermal contact resistance the material properties such as surface roughness and micro-hardness can be evaluated more accurately, rather than relying on values from literature. Also, the control of boundary conditions in experiments can be improved by better insulation techniques to eliminate the effects of convective heat transfer. In addition, a deeper study can be carried out to isolate the effect of each individual parameter to the value of contact resistance. The study can also be extended to more components. Finally, a further analysis can also be carried out on welded and oxidised surfaces, to get a trend of variation with degree of oxidation and the quality of the weld.

6 References

- [1] P. von Böckh and T. Wetzel, *Heat transfer: basics and practice*: Springer Science & Business Media, 2011.
- [2] A. K. Hasselström and U. E. Nilsson, "Thermal Contact Conductance in Bolted Joints," 2012.
- [3] M. Bahrami, M. M. Yovanovich, and J. R. Culham, "Thermal contact resistance at low contact pressure: Effect of elastic deformation," *International Journal of Heat and Mass Transfer*, vol. 48, pp. 3284-3293, 2005.
- [4] J. Greenwood and J. Williamson, "Contact of nominally flat surfaces," *Proceedings of the Royal Society of London. Series A. Mathematical and Physical Sciences*, vol. 295, pp. 300-319, 1966.
- [5] M. Cooper, B. Mikic, and M. Yovanovich, "Thermal contact conductance," *International Journal of heat and mass transfer*, vol. 12, pp. 279-300, 1969.
- [6] B. Mikić, "Thermal contact conductance; theoretical considerations," *International Journal of Heat and Mass Transfer*, vol. 17, pp. 205-214, 1974.
- [7] C. V. Madhusudana and C. Madhusudana, *Thermal contact conductance*: Springer, 1996.
- [8] F. Al-Astrabadi, P. O'Callaghan, and S. Probert, "Thermal resistance of contacts: Influence of Oxide films," *AIAA Paper*, 1980.
- [9] H. Zhao, A. J. Salazar, and D. P. Sekulic, "Analysis of fin-tube joints in a compact heat exchanger," *Heat Transfer Engineering*, vol. 30, pp. 931-940, 2009.
- [10] M. Yovanovich, "Micro and macro hardness measurements, correlations, and contact models," in *Collection of technical papers—44th AIAA aerospace sciences meeting*, 2006, pp. 11702-11729.
- [11] D. C. Timpe Jr, "Silicone Rubber Thermal Interface Materials: Applications and Performance Considerations."
- [12] M. Bahrami, M. Yovanovich, and E. Marotta, "Thermal joint resistance of polymer-metal rough interfaces," *Journal of electronic packaging*, vol. 128, pp. 23-29, 2006.
- [13] S. Parihar and N. Wright, "Thermal contact resistance of silicone rubber to AISI 304 contacts," *Journal of heat transfer*, vol. 121, pp. 700-702, 1999.
- [14] B. L. Moya, "Fluid and Thermodynamic Underhood Simulations."

Appendix A

Matlab Script to Estimate the Value of Thermal Contact Resistance

```
%% Thermal contact resistance
k_steel=19;
% k_steel= 52.019; % Thermal conductivity of steel in W/mK
k_steel= 0.875;
k_aluminum= 201.073; % Thermal conductivity of aluminum in W/mK
k_rubber=0.1558; % Thermal conductivity of rubber in W/mK
k_nylon=0.2994;
k_polyethylene=0.395;

% r_steel=; %average roughness steel
% r_aluminum=; %average roughness aluminum
% r_rubber=; % average roughness rubber

rms_roughness_steel=0.45*10^-6;
% rms_roughness_steel=0.125*10^-6;
rms_roughness_ssteel= 0.407*10^-6;
rms_roughness_aluminum=0.125*10^-6;
rms_roughness_rubber=2.4*10^-6;% In micro meters
rms_roughness_nylon=1.23*10^-6;
rms_roughness_polyethylene=1.92*10^-6;

% asperity_slope_steel=0.03;
asperity_slope_steel=0.04;
asperity_slope_ssteel=0.143;
asperity_slope_aluminum=0.03;
asperity_slope_rubber=1.9;
asperity_slope_nylon=0.2;
asperity_slope_polyethylene=0.24;

microhardness_steel= 3510; % in Mpa
microhardness_ssteel= 3800; % in Mpa
microhardness_aluminum= 1400; % in Mpa
microhardness_rubber= 560; % in Mpa
microhardness_nylon= 410; % in Mpa
microhardness_polyethylene= 410; % in Mpa

p=linspace(0.1,1,10);

%% TCR value of steel- steel contact

k_s= (2*k_steel*k_steel)/(2*k_steel);
rms_s= ((rms_roughness_steel^2+rms_roughness_ssteel^2)^0.5);
m_s= ((asperity_slope_steel^2+asperity_slope_ssteel^2)^0.5);
h_c= (((1.13*k_s*m_s)/rms_s)*((p./microhardness_steel).^0.94));
```

%% TCR value of stainless steel- aluminum contact

```
% k_s= (2*k_ssteel*k_aluminum)/(k_ssteel+k_aluminum);  
% rms_s= ((rms_roughness_ssteel^2+rms_roughness_aluminum^2)^0.5);  
% m_s= ((asperity_slope_aluminum^2+asperity_slope_ssteel^2)^0.5);  
% h_c= (((1.13*k_s*m_s)/rms_s)*((p./microhardness_aluminum).^0.94));  
%  
%% TCR value of steel- aluminum contact
```

```
% k_s= (2*k_steel*k_aluminum)/(k_steel+k_aluminum);  
% rms_s= ((rms_roughness_steel^2+rms_roughness_aluminum^2)^0.5);  
% m_s= ((asperity_slope_aluminum^2+asperity_slope_steel^2)^0.5);  
% h_c= (((1.13*k_s*m_s)/rms_s)*((p./microhardness_aluminum).^0.94));
```

%% TCR value of stainless steel- rubber contact

```
% k_s= (2*k_ssteel*k_rubber)/(k_ssteel+k_rubber);  
% rms_s= ((rms_roughness_ssteel^2+rms_roughness_rubber^2)^0.5);  
% m_s= ((asperity_slope_rubber^2+asperity_slope_ssteel^2)^0.5);  
% h_c= (((1.13*k_s*m_s)/rms_s)*((p./microhardness_rubber).^0.94));
```

%% TCR value of rubber - aluminum contact

```
% k_s= (2*k_aluminum*k_rubber)/(k_aluminum+k_rubber);  
% rms_s= ((rms_roughness_aluminum^2+rms_roughness_rubber^2)^0.5);  
% m_s= ((asperity_slope_rubber^2+asperity_slope_aluminum^2)^0.5);  
% h_c= (((1.13*k_s*m_s)/rms_s)*((p./microhardness_rubber).^0.94));
```

%% TCR value of Aluminum- Aluminum contact

```
% k_s= (2*k_aluminum*k_aluminum)/(2*k_aluminum);  
% rms_s= ((rms_roughness_aluminum^2+rms_roughness_aluminum^2)^0.5);  
% m_s= ((asperity_slope_aluminum^2+asperity_slope_aluminum^2)^0.5);  
% h_c= (((1.13*k_s*m_s)/rms_s)*((p./microhardness_aluminum).^0.94));
```

%% TCR value of steel- rubber contact

```
% k_s= (2*k_steel*k_rubber)/(k_steel+k_rubber);  
% rms_s= ((rms_roughness_steel^2+rms_roughness_rubber^2)^0.5);  
% m_s= ((asperity_slope_rubber^2+asperity_slope_steel^2)^0.5);  
% h_c= (((1.13*k_s*m_s)/rms_s)*((p./microhardness_rubber).^0.94));
```

%% TCR value of rubber- rubber contact

```
% k_s= (2*k_rubber*k_rubber)/(k_rubber+k_rubber);  
% rms_s= ((rms_roughness_rubber^2+rms_roughness_rubber^2)^0.5);  
% m_s= ((asperity_slope_rubber^2+asperity_slope_rubber^2)^0.5);  
% h_c= (((1.13*k_s*m_s)/rms_s)*((p./microhardness_rubber).^0.94));
```

%% TCR value of nylon- aluminum contact

```
% k_s= (2*k_nylon*k_aluminum)/(k_nylon+k_aluminum);
```

```
% rms_s= ((rms_roughness_nylon^2+rms_roughness_aluminum^2)^0.5);
% m_s= ((asperity_slope_aluminum^2+asperity_slope_nylon^2)^0.5);
% h_c= (((1.13*k_s*m_s)/rms_s)*((p./microhardness_nylon).^0.94));
```

```
%% TCR value of polyethylene- aluminum contact
```

```
% k_s= (2*k_polyethylene*k_aluminum)/(k_polyethylene+k_aluminum);
% rms_s= ((rms_roughness_polyethylene^2+rms_roughness_aluminum^2)^0.5);
% m_s= ((asperity_slope_aluminum^2+asperity_slope_polyethylene^2)^0.5);
% h_c= (((1.13*k_s*m_s)/rms_s)*((p./microhardness_polyethylene).^0.94));
```

```
%% TCR value of polyethylene- rubber contact
```

```
% k_s= (2*k_polyethylene*k_rubber)/(k_polyethylene+k_rubber);
% rms_s= ((rms_roughness_polyethylene^2+rms_roughness_rubber^2)^0.5);
% m_s= ((asperity_slope_rubber^2+asperity_slope_polyethylene^2)^0.5);
% h_c= (((1.13*k_s*m_s)/rms_s)*((p./microhardness_polyethylene).^0.94));
```

```
%% TCR value of polyethylene- polyethylene contact
```

```
% k_s= (2*k_polyethylene*k_polyethylene)/(k_polyethylene+k_polyethylene);
% rms_s=
((rms_roughness_polyethylene^2+rms_roughness_polyethylene^2)^0.5);
% m_s= ((asperity_slope_polyethylene^2+asperity_slope_polyethylene^2)^0.5);
% h_c= (((1.13*k_s*m_s)/rms_s)*((p./microhardness_polyethylene).^0.94));
```

```
%% TCR value of polyethylene- stainless steel contact
```

```
% k_s= (2*k_polyethylene*k_ssteel)/(k_polyethylene+k_ssteel);
% rms_s= ((rms_roughness_polyethylene^2+rms_roughness_ssteel^2)^0.5);
% m_s= ((asperity_slope_ssteel^2+asperity_slope_polyethylene^2)^0.5);
% h_c= (((1.13*k_s*m_s)/rms_s)*((p./microhardness_polyethylene).^0.94));
```

```
%% TCR value of stainless steel- steel contact
```

```
%
% k_s= (2*k_steel*k_ssteel)/(k_steel+k_ssteel);
% rms_s= ((rms_roughness_steel^2+rms_roughness_ssteel^2)^0.5);
% m_s= ((asperity_slope_steel^2+asperity_slope_ssteel^2)^0.5);
% h_c= (((1.13*k_s*m_s)/rms_s)*((p./microhardness_steel).^0.94));
```

```
%% TCR value of polyethylene- steel contact
```

```
% k_s= (2*k_polyethylene*k_steel)/(k_polyethylene+k_steel);
% rms_s= ((rms_roughness_polyethylene^2+rms_roughness_steel^2)^0.5);
% m_s= ((asperity_slope_steel^2+asperity_slope_polyethylene^2)^0.5);
% h_c= (((1.13*k_s*m_s)/rms_s)*((p./microhardness_polyethylene).^0.94));
```

```
%% TCR value of nylon- steel contact
```

```
% k_s= (2*k_nylon*k_steel)/(k_nylon+k_steel);
```

```

% rms_s= ((rms_roughness_nylon^2+rms_roughness_steel^2)^0.5);
% m_s= ((asperity_slope_steel^2+asperity_slope_nylon^2)^0.5);
% h_c= (((1.13*k_s*m_s)/rms_s)*((p./microhardness_nylon).^0.94));

%% TCR value of nylon- stainless steel contact

% k_s= (2*k_nylon*k_ssteel)/(k_nylon+k_ssteel);
% rms_s= ((rms_roughness_nylon^2+rms_roughness_ssteel^2)^0.5);
% m_s= ((asperity_slope_ssteel^2+asperity_slope_nylon^2)^0.5);
% h_c= (((1.13*k_s*m_s)/rms_s)*((p./microhardness_nylon).^0.94));

%% TCR value of stainless steel- stainless steel contact

% k_s= (2*k_ssteel*k_ssteel)/(2*k_ssteel);
% rms_s= ((rms_roughness_ssteel^2+rms_roughness_ssteel^2)^0.5);
% m_s= ((asperity_slope_ssteel^2+asperity_slope_ssteel^2)^0.5);
% h_c= (((1.13*k_s*m_s)/rms_s)*((p./microhardness_ssteel).^0.94));

%% TCR value of polyethylene- steel contact

% k_s= (2*k_polyethylene*k_steel)/(k_polyethylene+k_steel);
% rms_s= ((rms_roughness_polyethylene^2+rms_roughness_steel^2)^0.5);
% m_s= ((asperity_slope_steel^2+asperity_slope_polyethylene^2)^0.5);
% h_c= (((1.13*k_s*m_s)/rms_s)*((p./microhardness_polyethylene).^0.94));

%% TCR value of nylon- nylon contact

% k_s= (2*k_nylon*k_nylon)/(k_nylon+k_nylon);
% rms_s= ((rms_roughness_nylon^2+rms_roughness_nylon^2)^0.5);
% m_s= ((asperity_slope_nylon^2+asperity_slope_nylon^2)^0.5);
% h_c= (((1.13*k_s*m_s)/rms_s)*((p./microhardness_nylon).^0.94));

```

Appendix B

Matlab Script to Estimate the Value of Spreading Resistance at a Welded Joint

```
stag_dia=5*10^-3;
A_delta=pi*(stag_dia^2);
A_t=pi*(25^2);;
a=21*10^-3;
A_c=pi*(a^2);;
tau=((A_c/A_t)^0.5);
k=16;
if(tau<0.5)
    phi=(1-(1.4*tau));
else
    phi=(1-tau)^1.5;
end
r_s=((A_delta*phi)/(2*k*a));
```

Appendix C

Absolute temperatures for the Downpipe and Exhaust rubber for all the thermocouples.

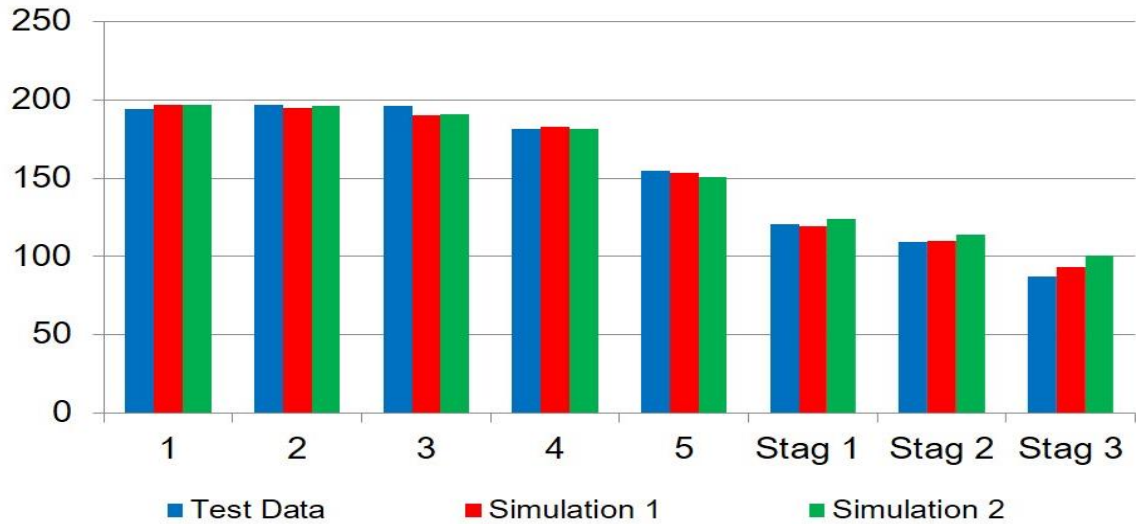


Figure C.1 Absolute temperatures for downpipe and stag interface for emissivity of 0.5 for two contact resistance values.

Simulation 1 : $R_c = 7e-4 \text{ m}^2 \text{ K/W}$ Simulation 2 : $R_c = 1e-4 \text{ m}^2 \text{ K/W}$

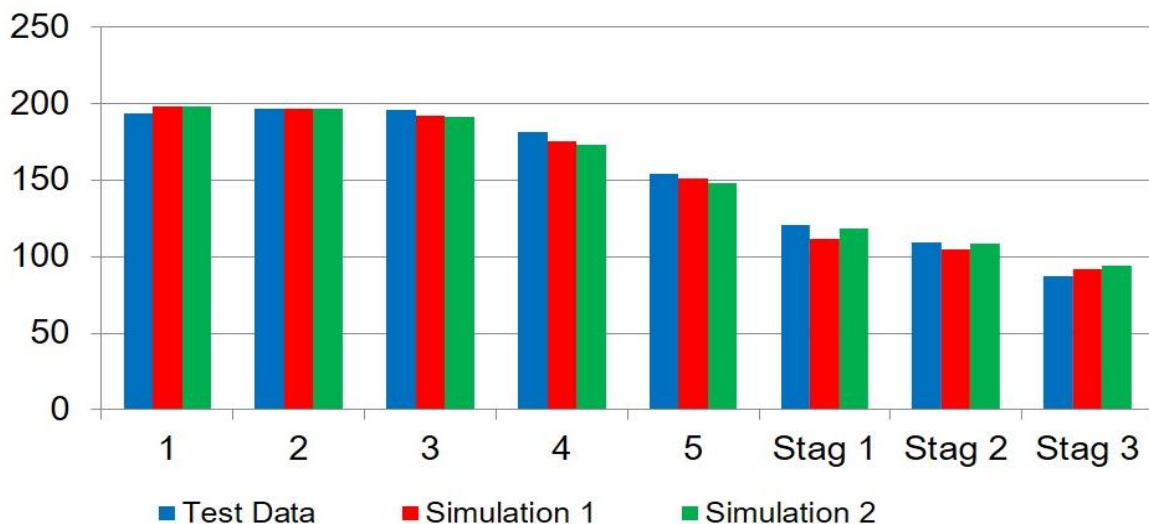


Figure C.2 Absolute temperatures for downpipe and stag interface for emissivity of 0.7 for two contact resistance values.

Simulation 1 : $R_c = 7e-4 \text{ m}^2 \text{ K/W}$ Simulation 2 : $R_c = 1e-4 \text{ m}^2 \text{ K/W}$

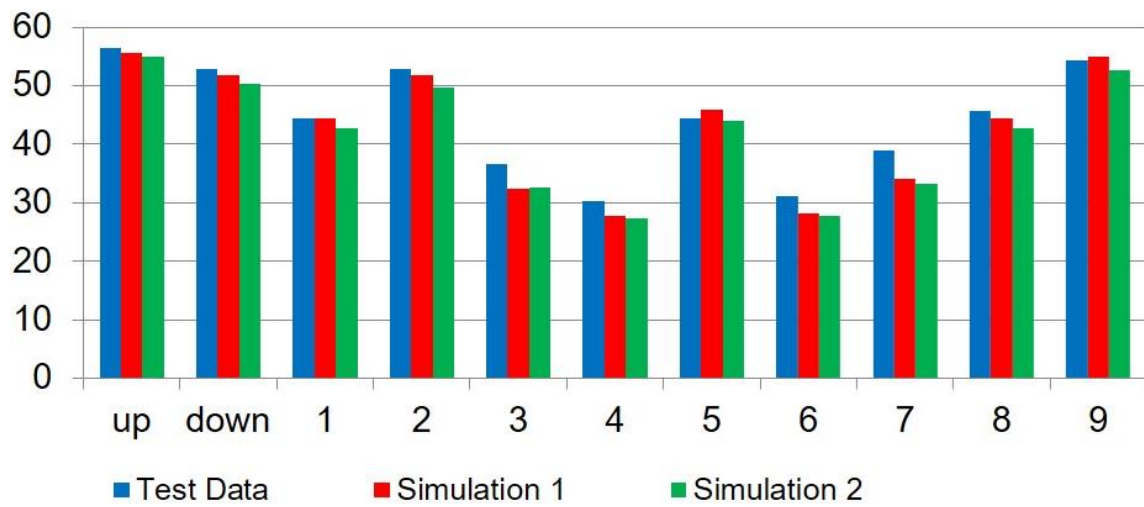


Figure C.3 Absolute temperatures for stag and rubber interface for emissivity of 0.5 for two contact resistance values.

Simulation 1 : $R_c = 0.012 \text{ m}^2 \text{ K/W}$

Simulation 2 : $R_c = 0.021 \text{ m}^2 \text{ K/W}$

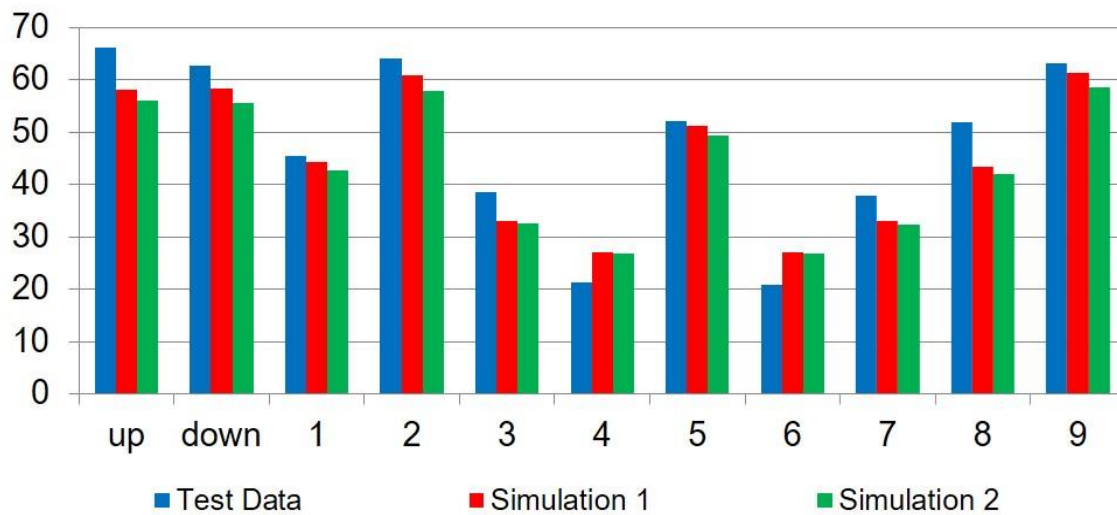


Figure C.4 Absolute temperatures for stag and rubber interface for emissivity of 0.7 for two contact resistance values.

Simulation 1 : $R_c = 0.012 \text{ m}^2 \text{ K/W}$

Simulation 2 : $R_c = 0.021 \text{ m}^2 \text{ K/W}$

Appendix D

Absolute temperatures for the Heat Shield for all the thermocouples.

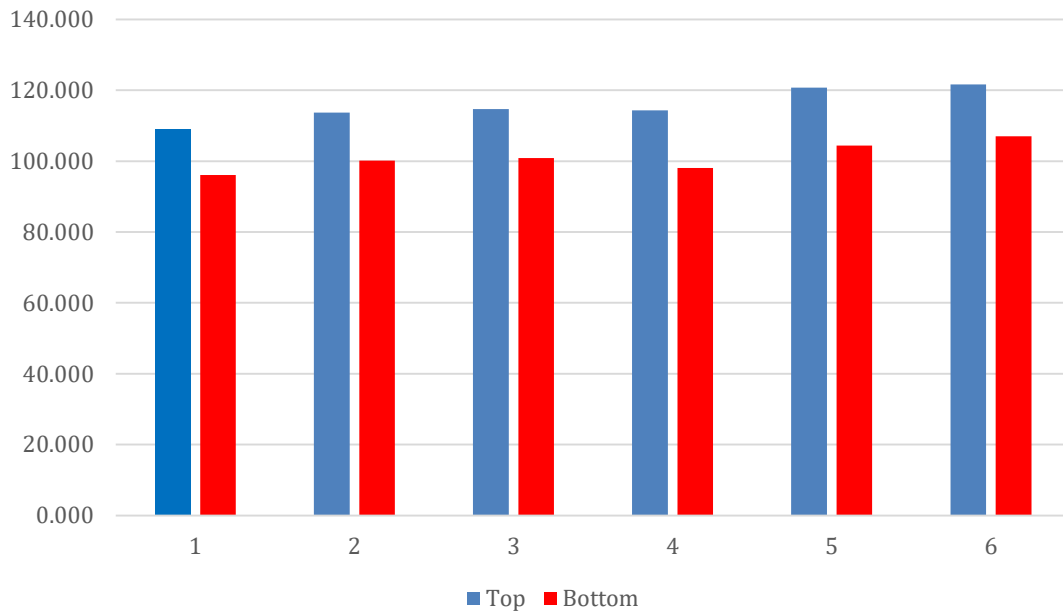


Figure D.1 Absolute temperatures at the different thermocouples on the heat shield after 7 minutes in experiments

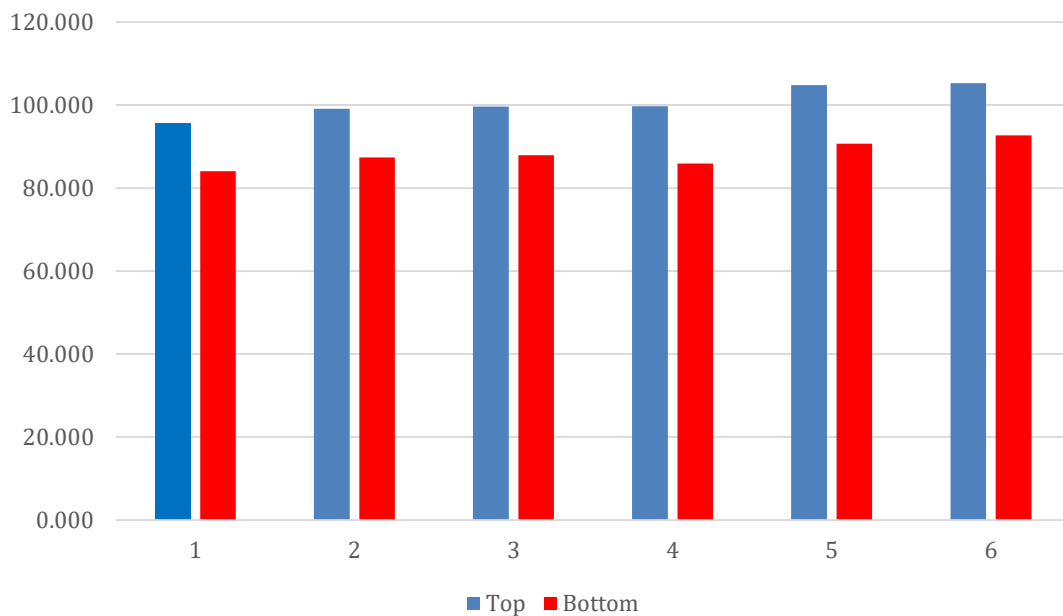


Figure D.2 Absolute temperatures at the different thermocouples on the heat shield after 8 minutes in experiments

Appendix E

Absolute temperatures for the powertrain mount for all the thermocouples.

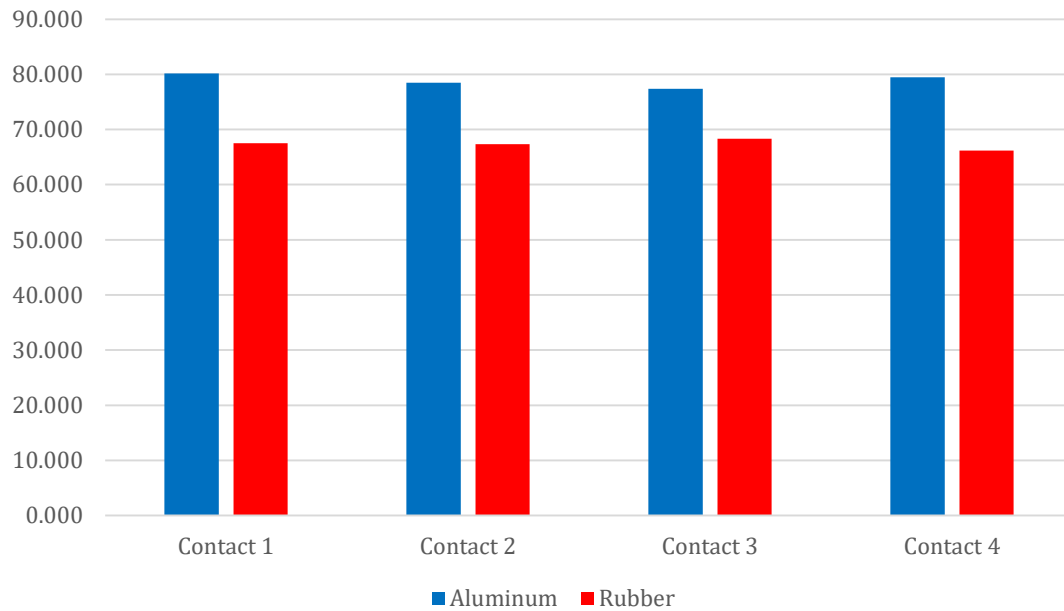


Figure E.1 Absolute temperatures for the powertrain mount – Experimental data

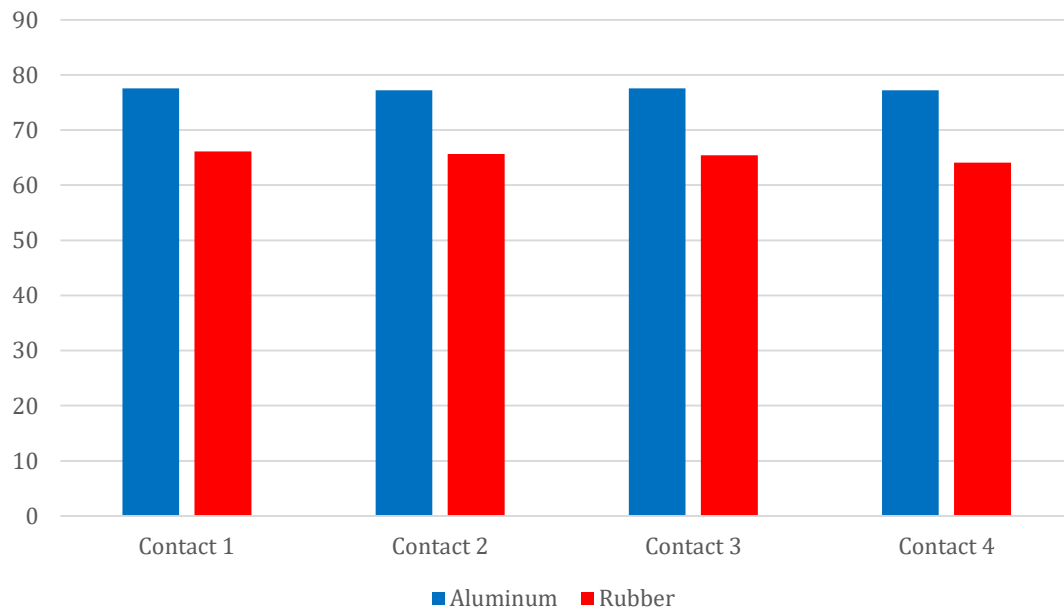


Figure E.2 Absolute temperatures for the powertrain mount – Simulation data

Default case $R_c = 0.021 \text{ m}^2 \text{ K/w}$

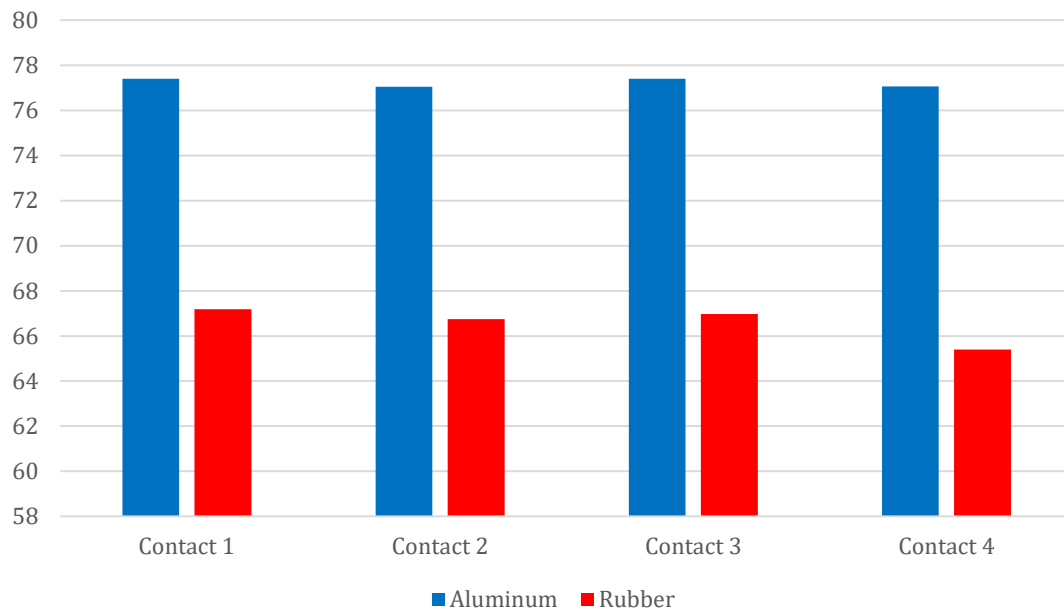


Figure E.3 Absolute temperatures for the powertrain mount – Simulation data
Changed case $R_c = 0.012 \text{ m}^2 \text{ K/w}$